İSTANBUL TECHNICAL UNIVERSITY ★ INSTITUTE OF SCIENCE AND TECHNOLOGY

MODELING DIESEL ENGINE OIL CONSUMPTION AND COMPARISON WITH EXPERIMENTAL DATA

M.S. Thesis by
Göktan KURNAZ, B.Sc.

Department : **Mechanical Engineering**

Programme: **Dynamics, Vibrations and Acoustics of Machinery**

Supervisor : Assist. Prof. Dr. Özgen AKALIN

June 2007

İSTANBUL TECHNICAL UNIVERSITY ★ INSTITUTE OF SCIENCE AND TECHNOLOGY

MODELING DIESEL ENGINE OIL CONSUMPTION AND COMPARISON WITH EXPERIMENTAL DATA

M.S. Thesis by
Göktan KURNAZ, B.Sc.
(503041404)

Date of Submission : 7 May 2007
Date of Defense Examination: 15 June 2007

Supervisor (Chairman): Assist. Prof. Dr. Özgen AKALIN

Members of the Examining Committee: Prof.Dr. Metin GÜRGÖZE (İTÜ)

Prof.Dr. Mustafa ÜRGEN (İTÜ)

June 2007

İSTANBUL TECHNICAL UNIVERSITY ★ INSTITUTE OF SCIENCE AND TECHNOLOGY

DİZEL MOTOR YAĞ TÜKETİMİNİN MODELLENMESİ VE DENEYSEL VERİLERLE KARŞILAŞTIRILMASI

Yüksek Lisans Tezi
Müh. Göktan KURNAZ
(503041404)

Tezin Enstitüye Verildiği Tarih : 7 Mayıs 2007

Tezin Savunulduğu Tarih: 15 Haziran 1997

Tez Danışmanı: **Y. Doç. Dr. Özgen AKALIN**

Diğer Jüri Üyeleri: **Prof.Dr. Metin GÜRGÖZE (İTÜ)**

Prof.Dr. Mustafa ÜRGEN (İTÜ)

Haziran 2007

ACKNOWLEDGEMENTS

I would like to express my sincere appreciation to Assist. Prof. Dr. Özgen AKALIN for his guidance throughout the research.
Special thanks to Ford Otomotiv Sanayi A.Ş. for sponsoring this project and especially to Ömer Rüştü ERGEN for his encouragement and guidance.
I also would like to thank to Osman Taha Şen and Özcan Gül for their kind support throughout the project.
Last but not least, I would like to express my deepest thanks to my family for their great patience, understanding and support to the preparation of this thesis.

TABLE OF CONTENTS

LIST OF ABBREVIATIONS

PFP	: Peak Firing Pressure
TS	: Thrust Side
ATS	: Anti-thrust Side
TDC	: Top Dead Centre
CA	: Crank Angle
ECU	: Electronic Control Unit

LIST OF TABLES

LIST OF FIGURES

LIST OF SYMBOLS

m_p : Piston mass

I_p : Piston moment of inertia around pin center

F_g : Weight of piston

F_{gas} : Force due to combustion pressure

F_r : Piston ring contact force

F_{ci} : Liner contact force at thrust and anti-thrust sides at i'th cross section

F_{pin} : Force exerted by piston pin on piston

M_{ci} : Moment due to piston-liner contact at i'th cross section

M_g : Moment due to piston weight

M_{gas} : Moment due to gas force (active when the combustion chamber is non-symmetric)

M_r : Moment due to ring axial and radial contact force

M_p : Moment due to friction at piston pin

$\ddot{\kappa}$: Angular acceleration of piston

m_r : Mass of piston ring

$F_{fric,ax}$: Friction between liner and ring surface

$F_{gas,ax}$: Gas force

$F_{hydr,ax}$: Axial damping force caused by the oil filling of the groove

F_{bend} : Bending force caused by the interaction between TS and ATS

$F_{tension}$: Force caused by the tension of the ring

$F_{gas,rad}$: Radial gas force

$F_{fric,rad}$: Friction force between ring and ring groove

$F_{hydr,rad}$: Force caused by the hydrodynamic gap between liner and ring running face

$M_{elastic}$: Elastic bending moment due to ring twisting

$M_{pre-twist}$: Elastic moment due to pre-twist angle

h_i : Moment arm for each force component

p_c : Chamber pressure

T_c : Chamber temperature

V_c : Chamber volume

p_o : Surrounding or neighboring chamber pressure

T_o : Surrounding or neighboring chamber temperature

V_o : Neighboring chamber volume

R : Gas constant of combustion gas

k : Isentropic exponent

Δt : Time step

h : Nominal film thickness

$\overline{h}_T$: The average gap

$\overline{p}$: Mean hydrodynamic pressure

σ : Composite surface roughness

Φ_x : Pressure flow factor

Φ_s : Shear flow factor

U : Sliding velocity

β : Mass transfer coefficient

c_{film} : Concentration of lube oil at film surface

c_∞ : Concentration of lube oil in combustion chamber

$\dot{m}$: Mass flow rate into boundary surface

y : Coordinate perpendicular to boundary surface

Δs : Movement of the piston during time step Δt

s_{film} : Uncovered area of the oil film

a_0 : Acceleration at the beginning of motion

h_{film} : Height of oil film between top land and liner

d_{film} : Diameter of oil film

$\dot{m}_t^{oil}$: Oil consumption at time t

$\dot{m}_t^{fuel}$: Fuel mass flow rate at time t

$\dot{m}_t^{Air}$: Air mass flow at time t

$[S]_t^{Oil}$: Sulfur concentration of oil

$[S]_t^{Fuel}$: Sulfur concentration of fuel at time t

$[S]_t^{Air}$: Sulfur concentration of air at time t

$[S]_t^{Exh}$: Sulfur concentration in exhaust gas at time t

DİZEL MOTOR YAĞ TÜKETİMİNİN MODELLENMESİ VE DENEYSEL VERİLERLE KARŞILAŞTIRILMASI

ÖZET

Dizel motor yağ tüketimi iki temel sebepten dolayı otomotiv mühendisliğinde ilgi duyulan bir konu haline gelmiştir. Öncelikle, doğal kaynakların korunması amacıyla egzoz emisyon limitleri günden güne aşağı çekilmekte ve bu nedenle özellikle motor geliştime alanındaki mühendislik gücünün büyük bölümü egzoz yönetmelikleri ile uyum için kullanılmaktadır. İkinci olarak, kullanıcının günümüz yüksek teknolojili motorlarından beklentisi günden güne artmakta ve yağ tüketimi önemli bir kriter olarak değerlendirilmektedir. Özellike ağır hizmet tipi dizel motorlarda yağ tüketiminin ve dolayısıyla işletme maliyetlerinin nispeten daha yüksek olması nedeniyle, yağ tüketimi kullanıcı memnuniyeti açısından daha önemli olmaktadır. Bu nedenle, yağ tüketimi üzerinde etkili olan faktörlerin belirlenmesi ve anlaşılması oldukça önem arz etmektedir.

Bu çalışmada, bir ağır hizmet dizel motor için piston dinamiği, segman dinamiği ve yağ tüketim modeli oluşturulmuştur. Bu model kullanılarak, tepe silindir basıncının piston dinamiği, segman dinamiği ve sonuç olarak motorun yağ tüketimi üzerindeki etkileri belirli sabit rejim çalışma noktalarında incelenmiştir. Yapılan simülasyonlarda ölçülen silindir içi basınç eğrileri kullanılmıştır. Bu çalışma noktalarında farklı silindir basınç karakteristikleri denenirken, motor dönme hızı ve çıkış yükü sabit tutulmuştur. Ayrıca motorun anlık yağ tüketimi farklı silindir basınçları ile SO_2 izleme yöntemi ile ölçülmüş ve teorik modelden elde edilen bulgularla deneysel veriler kıyaslanmıştır. Tepe silindir basıncının piston ve segman dinamiği üzerinde oldukça etkili olduğu görülmüş fakat yağ tüketimi üzerinde önemli bir değişiklik yaratmadığı gözlenmiştir.

MODELLING DIESEL ENGINE OIL CONSUMPTION AND COMPARISON WITH EXPERIMENTAL DATA

SUMMARY

Diesel engine oil consumption has been a major interest to automotive engineering because of two main reasons. Firstly, the exhaust emission regulations are being more stringent in order to preserve the environment, and consequently, most of the engineering labor in engine development is spent to comply with those legislations. Secondly, user expectations from the recent high technology engines are becoming higher everyday and any considerable disadvantage in oil consumption is considered to be a weakness. Oil consumption is even more effective on customer satisfaction for heavy-duty diesel engines, since oil consumption and operational costs of those engines are also higher. Therefore, identification and understanding of factors influencing oil consumption has been an important subject.

In this study an integrated analytical piston dynamics, ring dynamics and lube oil consumption model is established for a heavy-duty diesel engine. Measured in-cylinder pressure curves are used as input for the simulations. Using this model, the effect of cylinder peak firing pressure on piston dynamics, ring dynamics and finally on oil consumption is investigated at certain steady state operating conditions. Torque and speed are kept constant while the cylinder pressures are varied during the investigation. The oil consumption of the engine is also measured using SO_2 tracing technique for different peak firing pressures and a comparison is made between analytical findings and acquired data. Peak firing pressure is found to be an effective parameter for piston and ring dynamics but significant effect on oil consumption is not observed.

1. INTRODUCTION

Engine oil consumption is recognized as one of the most important criteria for modern internal combustion engine performance and, consequently, customer satisfaction. Engine oil consumption is also recognized to be a significant source of pollutant emissions in automotive engines. Unburned or partially burned oil in the exhaust gases contributes directly to hydrocarbon and particulate emissions. Moreover, chemical compounds in oil additives can poison exhaust gas treatment devices and can severely reduce their conversion efficiency. As a part of the effort to comply with increasingly stringent emission standards, engine manufacturers strive to minimize engine oil consumption. This requires the advancement of the understanding of the characteristics, sources, and driving mechanisms of oil consumption. Enough lubricating oil must be provided to the upper ring pack region to prevent dry running and limit friction and wear, but any excess oil will become consumed and contribute to unnecessary oil consumption.

The high efficiency, high power density turbo-charged inter-cooled direct injection engines have higher combustion pressures and thermal loading, and they are continuously replacing spark ignition engines. Therefore, oil consumption issue becomes more challenging for today's automotive engineering.

The inherent complexities in power cylinder system and large amount of testing cost and time necessitates analytical tools which enables engineers to optimize their design prior to any prototype build and testing. This requires the advancement of the understanding of the characteristics, sources, and driving mechanisms of oil consumption. Such an analytical model does not only provide early predictions for power cylinder performance but also provides a means for the identification and prevention of failure modes.

The modern direct injection turbo charged diesel engines owe their high thermal efficiency to the utilization of high cylinder pressures (up to 220 bar). It is now a quite well known fact that engine efficiency (It is reported by **Rakopoulos et. al. (2201)** that

effect of peak firing pressure on engine friction is not significant) increases as peak cylinder pressure increases. Unfortunately, there are many other factors influenced by cylinder pressure which drives the engine management strategy to a trade off among those. The trade off between nitrous oxides and BSFC (Brake Specific Fuel Consumption) is the most frequently encountered compromise and, therefore, there are a large amount of studies for the effect of peak cylinder pressure on diesel emissions, especially nitrous oxides. However, no studies have been found which investigates the effect of peak firing pressure on diesel engine oil consumption.

Peak cylinder pressure or engine calibration has been one factor which is tried to be kept constant when investigating the effect of any parameter on oil consumption, to prevent it being a lurking variable in analysis. The main focus of this study is to first explore, than quantify the effects of peak cylinder pressure on diesel engine oil consumption at various operating points, while other significant parameters such as load (or brake mean effective pressure), oil temperature and speed are kept constant.

Firstly, an oil consumption model has been established by using AVL Glide software and various parameters in the model has been adjusted to match predicted blow-by levels with measured data to increase the accuracy of the model. Then, effect of peak cylinder pressure has been investigated by real-time oil consumption measurement using SO_2 tracing technique and online engine calibration. Finally, the mechanisms behind observed variability on oil consumption are analyzed with the help of available analytical model.

This thesis report consists of 6 sections including the introduction. In section 2, a literature survey is given, also comprising of oil consumption mechanisms, piston dynamics and ring dynamics. Basic oil consumption sources and driving mechanisms are presented with previously published work. Piston secondary motion is explained with various calculation approaches and its effects on ring dynamics and consequently oil consumption are presented. At the end of the section 2, previous work on ring dynamics is presented together with detailed descriptions of basic characteristics of ring motion and possible failure modes. Section 3 includes general information about the AVL Glide, which is used for analytical investigations in this study. Basic principles,

governing equations and common assumptions employed in the calculation models are presented. Section 4 is the main focus of the thesis which concentrates on the effects of peak firing pressure on diesel engine oil consumption. The findings from the analytical model are compared with experimental results and necessary explanations are made clarifying the differences, explaining the trends and underlying mechanisms.

2. PISTON DYNAMICS, RING DYNAMICS AND OIL CONSUMPTION, A LITERATURE SURVEY

2.1. Oil Consumption Mechanisms in Diesel Engines

The definition of "oil consumption" is worth doing at the beginning of this text, because, for the end user, oil consumption may be treated as the degradation of oil which needs to be replaced in oil change intervals. Therefore the aeration, oxidation and other lube oil degrading mechanisms are significant. However, in the context of this study, oil consumption is referred as the amount of lube oil that is directly transported into the exhaust stream and carried out of the engine. The variation in chemical properties and consequently the variation in the ability of the oil to make its functions are not considered. Furthermore, being the major source of oil consumption, oil consumption in the power cylinder is in the scope of the text and other oil consumption due to valve stem seal and turbocharger is ignored.

Significant amount of research has been made to identify and classify oil consumption sources in internal combustion engines. Mainly four potential oil consumption sources have been identified to contribute to total engine oil consumption during operation **(Yılmaz et. al., 2004)**:

1. Oil throw-off from the top compression ring
2. Transport of oil with reverse gas flow into the combustion chamber
3. Evaporation of oil from the liner wall
4. Oil scraping by piston top land

These oil consumption mechanisms are explained in detail below.

2.1.1. Oil throw-off from top compression ring

It has been suggested and supported by experimental data that liquid oil accumulated above the top compression ring can be transported into the combustion chamber as a result of inertia forces during acceleration and deceleration of piston assembly (see Figure 2.1).

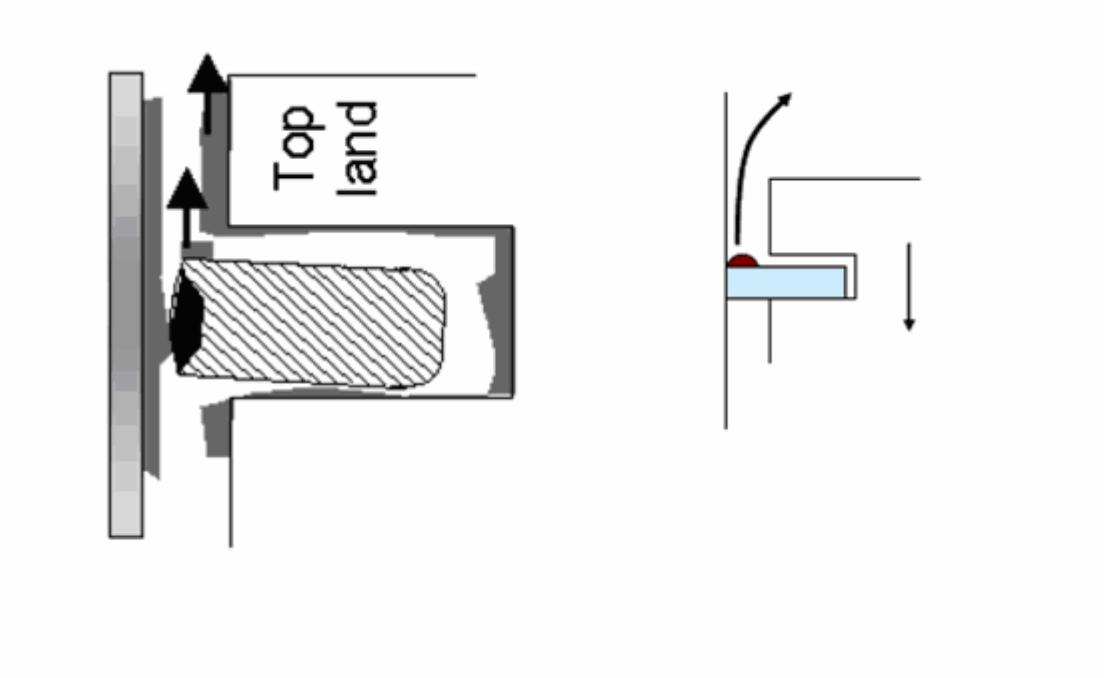

Figure 2.1: Oil Throw-off from Top Ring

The importance of this driving mechanism is believed to depend on accumulated oil film on the top land and top ring. Oil throw-off was visualized in research with single cylinder engine spark ignition engine at low load conditions **(Inagaki et. al., 1995, Thirouard et. al., 1998)** .

2.1.2. Transport of oil with reverse gas flow into the combustion chamber

During some part of the piston stroke gas pressure in the second land may be higher than gas pressure in the combustion chamber. This pressure gradient may drive the reverse flow of gas into the combustion chamber through the top ring gap and through the ring groove if the top ring looses its stability **(see Figure 2.2).** This transported oil may be both in liquid or mist form. This phenomenon is also visualized during engine operation at low load **(Nakashima et. al., 1989)**.

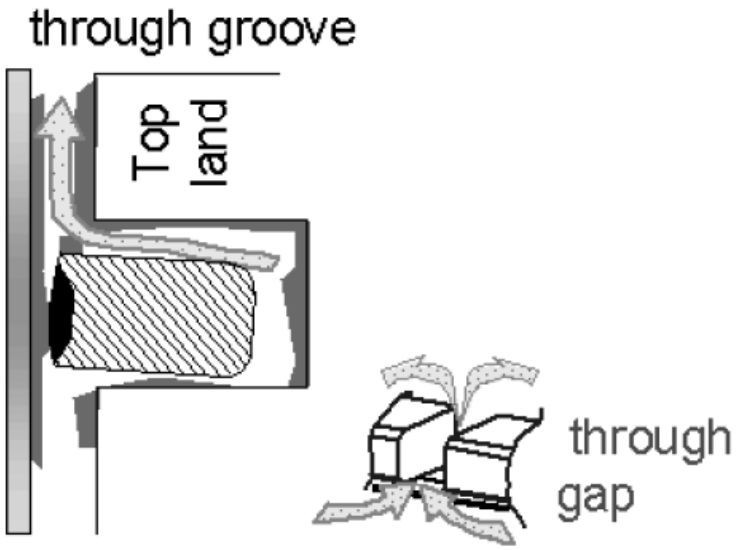

Figure 2.2: Oil Consumption by Reverse Gas Flow

Yoshida et. al. (1995) have also made theoretical studies supported by measurements and shown that blow-up gas into the combustion chamber is significantly concerned with oil consumption.

2.1.3. Evaporation of oil from the liner wall

Oil evaporation from the liner wall was also found to contribute to engine oil consumption. One of the most complete models presented thus far is by **Wahiduzzaman et al (1991)**. At its core, their model treats oil vaporization as the diffusion of oil vapor through a gas boundary layer on the cylinder's surface. The oil itself is modeled as being composed of several distinct hydrocarbon species each with its own boiling point and associated vapor pressure. Overall oil vaporization is computed by computing the local instantaneous oil vapor mass flux for numerous locations on the liner, integrating over time and space, and summing over the number of oil species. For the heavy-duty diesel engine that they modeled, their results show that contribution of oil vaporization to overall oil consumption is small (2-5%). They found that oil consumption was sensitive to oil grade and cylinder temperature. Interestingly, their model also showed that under

certain conditions most of the oil vaporization occurs during the non-firing half of the engine cycle.

Audette and Wong (1999) have developed a similar model to Wahiduzzaman's, extending the model capability to consider variation of oil composition along the liner. They have found the same result that most of the oil vaporization takes place during compression and intake strokes and they attributed this to low sensitivity of oil film surface temperature to bulk gas temperature. The thermophysical properties of ideal air at compression and expansion strokes are also found to cause this result. They reported that vaporization rate is strongly dependent on liner temperature and oil composition.

It is worth noting that all the approaches aiming to model oil evaporation rely on a ring dynamics model to predict the local oil film thickness on the liner. Therefore, piston ring lubrication has also direct influence on predicted oil vaporization by governing the left oil film thickness on the liner.

2.1.4. Oil scraping by piston top land

The top land clearance of a piston is rather low under engine running conditions. Deposits on the top land and lateral motion due to piston secondary movement cause contact with the liner wall. At each upward stroke, the piston top edge scrapes along the liner wall and pushes oil into the combustion chamber **(see Figure 2.3).**

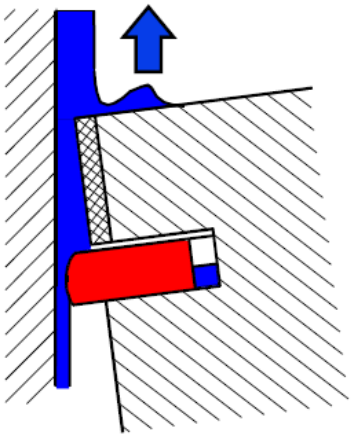

Figure 2.3: Topland Oil Scraping

2.2. Piston Dynamics and Its Effects on Oil Consumption

The motion of the internal combustion engine piston has a great influence on main attributes of an internal combustion engine such as fuel consumption, blow-by, oil consumption, wear and noise emission. Therefore a large amount of research has been made to understand the basic characteristics of piston motion. In this study, piston motion is mostly considered with the secondary motion, i.e. the tilting and transverse movement of the piston in the cylinder bore, in view of its effects on piston ring dynamics and consequently on blow-by and oil consumption. Although the majority of work on piston dynamics addresses the issue of friction between piston skirt and liner and the slap occurring as a result of collusion between piston and liner, friction and piston slap are not directly assessed in thesis as it is mainly focused on oil consumption.

2.2.1. Piston secondary motion

The primary motion of the piston in a reciprocating engine is the oscillatory movement of the piston parallel to the axis of the cylinder. This motion is a result of the rotation of the crankshaft and the coupling between the crankshaft and the piston via the connecting rod and the piston pin. The primary motion of the piston is governed by the kinematics of the ideal slider crank mechanism as a single degree of freedom system.

The secondary motion of the piston, on the other hand, exists as a result of the deviation of the slider crank mechanism from ideal conditions. The finite clearances in the revolute joints, i.e. the joints between connecting rod and crankpin and between the piston pin and pin bore, additionally the finite clearances in the piston-cylinder pair, the friction between the piston and liner and the uneven mass distribution of the piston results in piston motion perpendicular to the liner axis in thrust plane (plane normal to the pin axis) and also rotational motion about the pin center, relative to the cylinder axis. This motion is demonstrated in **Figure 2.4**. Therefore, piston secondary motion is described as any motion of the piston apart from the motion of the slider, governed by the kinematics of the ideal slider-crank mechanism.

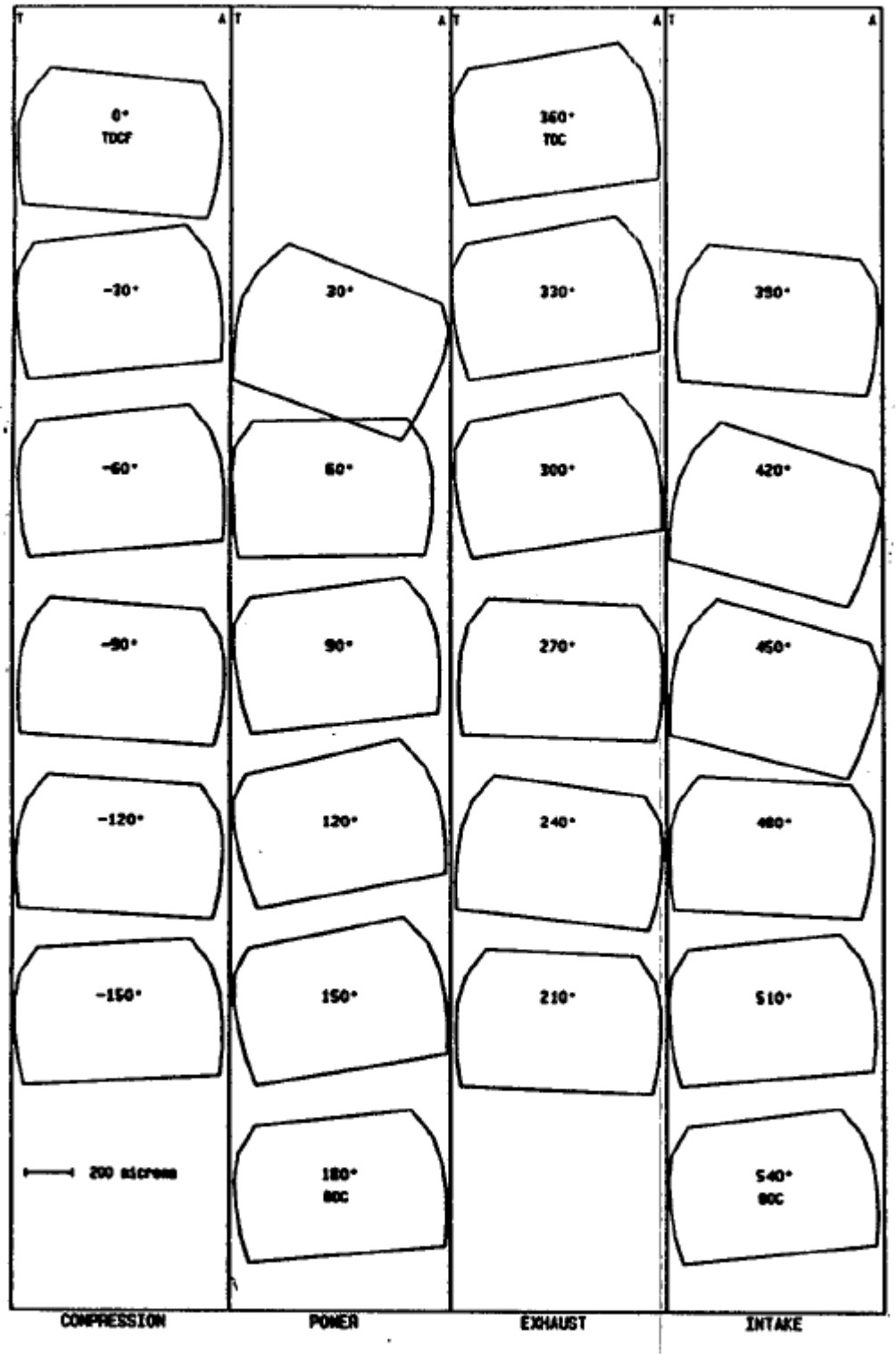

Figure 2.4: Piston Secondary Motion during One Engine Cycle **(Keribar et. al., 1993)**

The oil film between the liner and piston skirt (in all piston dynamics studies the only contact between the piston and liner is assumed to occur from the skirt, brought by the assumption that the piston design is proper, i.e. there is no contact through the piston crown), the mass distribution of the piston-ring pack or the location of the center of mass of the piston assembly, the piston pin offset, overall piston dimensions, crankshaft dynamics, elasticity of components and gas forces due to the combustion in the cylinder are all effective on piston dynamics.

The effects of pin location, radial clearance, oil viscosity and operating conditions on piston stability in a small ringless hermetic reciprocating compressor used in refrigerators has been investigated by **Prata et. al. (2000).** Because of the ringless design oil consumption and efficiency of the compressor was directly related to piston motion. The oil film behavior around the circumference of the piston was determined by solving Reynold's 2-D equations and effect of radial clearance has been investigated to find an optimum clearance for lowest friction and lowest gas leakage.

Keribar et. al. (1993) established and integrated model of piston motion which is comprised of coupled models of piston secondary dynamics, skirt oil film elastohydrodynamic lubrication and wristpin bearing hydrodynamics, developed earlier by the authors **(Dursunkaya and Keribar, 1992).** Models have been further expanded to calculate distributions of cumulative load on the skirt and cylinder, which causes wear, and to account for details of skirt and crankcase geometry. The skirt elasticity model has also been improved to account for the effects of piston crown and pin boss stiffness in conventional, one-piece pistons. They applied their model to investigate the effect of design and operating parameters (piston stiffness and mass, engine speed and load, skirt/cylinder temperatures and thermal deformations, skirt-cylinder cold clearance and pin offset) on the behavior of an automotive piston.

Tian et. al. (1994) established a model which predicts piston motion with partially-flooded skirts in mixed lubrication. This is an important advantage in piston slap analysis since the simplistic assumption of a fully-flooded skirt is too rigid, especially when the actual oil film is thin. This model incorporates, as before, the effects of piston skirt surface waviness, roughness, axial surface profile, bulk elastic deformation and

thermal distortion, lubrication and friction. However, the modified model has also been integrated with a ring-pack model where axial friction forces between the ring faces and the liner, as well as sidewise frictional forces between the rings and ring groove surfaces, have been included. They used their model to predict impact force of the piston on the liner, which is the source of excitation of piston slap. Than, they have used their model for piston skirt profile optimization and investigate the effect of liner deformation.

2.2.2. Effect of piston secondary motion on lube oil consumption

This study is mainly concerned with the oil consumption rather than friction and lubrication conditions. The effect of piston dynamics on friction and lubrication is obvious; however, the influence on lube oil consumption is worth noting here. The piston secondary motion is known to affect lube oil consumption in following ways:

1. The lateral and tilting movement of the piston results in a variable piston-liner clearance around the circumference of the piston. Mostly the effect of converging-diverging properties of the ring lands as a result of piston tilting is ignored to avoid too much complexity and the lateral motion is considered in flow area calculations. This effect is covered in detail in Section 2.3.
2. The tilting motion of the piston also affects the running profile of the piston ring and creates an unbalanced radial force distribution which have great significance on oil film thickness and therefore oil consumption **(Tian and Wong, 2000). Figure 2.5** demonstrates this situation for a three piece oil control ring.

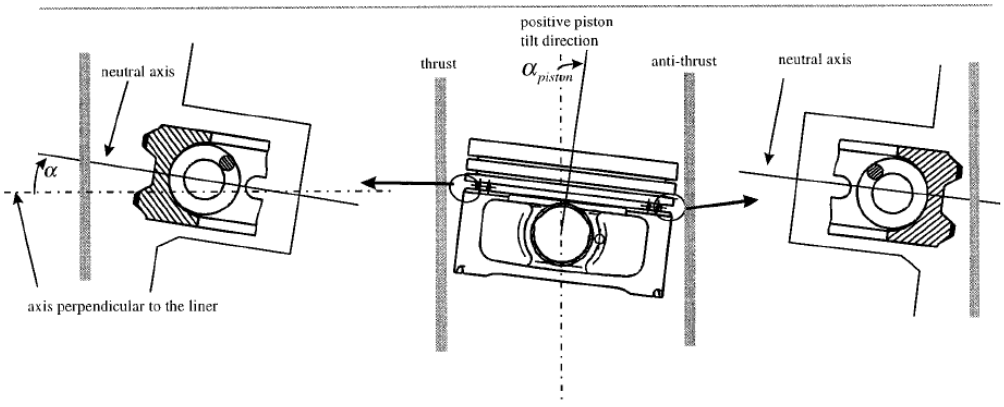

Figure 2.5: Piston Tilting Effect on Ring Twist **(Tian and Wong, 2000)**

3. The amount and sense of tilting of the piston determines the mode of contact between the piston ring and the ring groove, whether it is inner or outer contact as shown in **Figure 2.6**. **Rabuté and Tian (2001)** suggested a positive twist angle by means of an inner chamfer on top ring to obtain inner diameter sealing configuration and reported that a decrease in blow-by has been observed. See also references for more information **(Mihara and Inoue, 1995).**

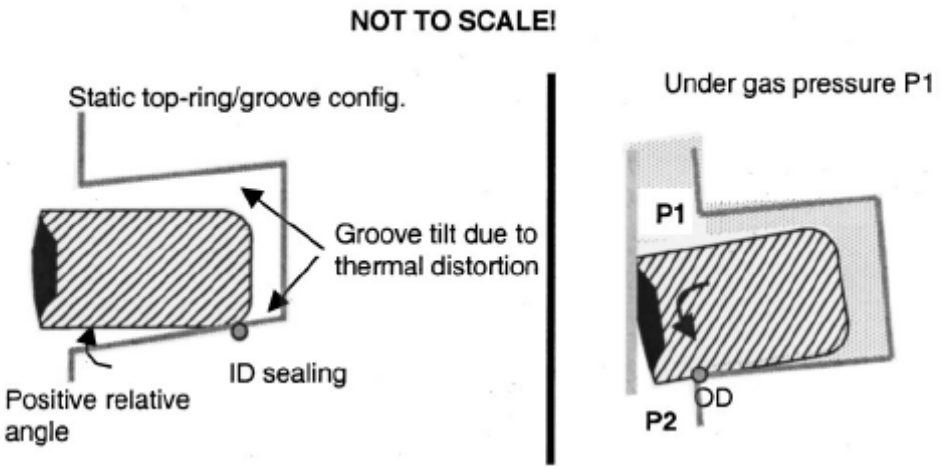

Figure 2.6: Different Modes of Contact Due To Piston Tilting and Ring Twist (**Rabuté and Tian, 2001)**

2.3. Piston Ring Dynamics and Its Effects on Oil Consumption

Similar to the case in reciprocating piston, the global or primary motion of the piston ring is governed by the slider-crank kinematics and is the same as the piston movement. However, wear of piston-ring-liner system, oil consumption and blow-by is mostly affected by ring axial movement relative to the ring groove and twisting around the center of ring cross section.

Figure 2.7 shows the forces and moments acting on the piston ring due to gas pressure, inertia effects and interaction with the piston groove and liner or oil film depending on the contact regime.

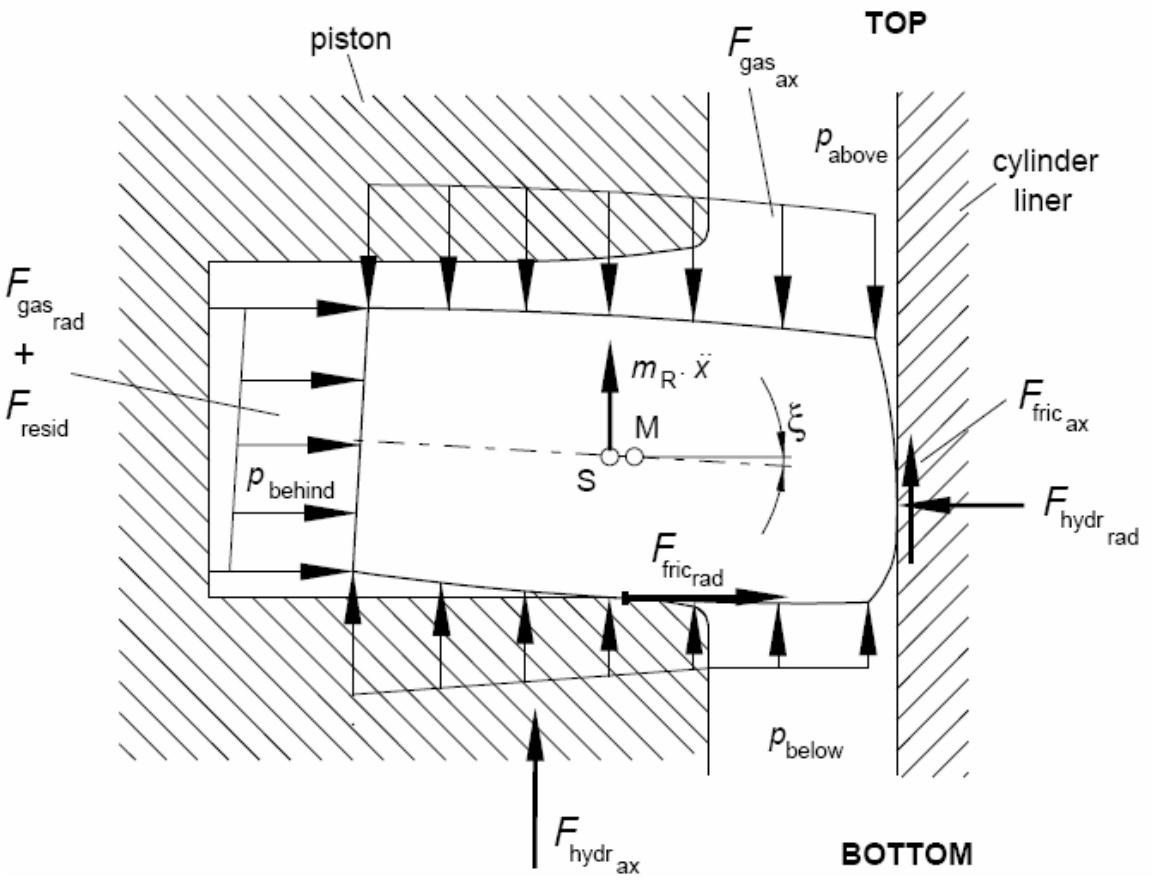

Figure 2.7: Forces Acting on a Piston Ring

A great amount of research has been made for modeling friction in piston ring-liner system. However, since the main concern is the friction and wear rather than oil and gas transport, most of these studies ignore the secondary movement of the piston ring. There are a limited number of research on piston ring dynamics and its effects on oil consumption. The difficulty in piston ring dynamics calculations is the combined effects of fluid, gas dynamics and elastic bodies. A relatively good estimation of piston ring motion not only requires the solution of equations of motion but also a precise model for gas pressures in the ring lands and grooves.

Yoshida et. al. (1993) has investigated the effect of pressure balancing both experimentally and by using Furuhama's theory **(Furuhama and Hiruma, 1979)**. Their model was mainly focused on pressure conditions ignoring the dynamics in the calculations. They found close results between measurements and calculations and have

shown that choosing second ring gap larger than first ring gap and increased second land volume reduce speed of second ring lifting off and prevent top ring from lifting off.

Mihara and Inoue (1995) experimentally investigated the effect of different top ring designs on oil consumption. Their study showed that top ring keystone angle and top ring running profile have high influence on engine oil consumption.

Nakashima and Ishihara (1995) investigated the effects of the positions of the piston ring gaps, the end clearance size and the shape of the piston ring gaps on the lubricating oil flow into the combustion chamber. They reported that main stream of the lubricating oil flow goes from the lower ring gap to the upper ring gap in all of the positions of the piston ring gaps and that the position of the oil ring upper side rail gap has a great influence on the lubricating oil flow.

The piston rings operate under the action of the forces above; however, the gas and inertia forces are those which determine the fundamental characteristics of piston ring motion. The influence of friction and damping is limited to shifting general trends of ring motion, since their magnitudes are much smaller compared to gas and inertia forces.

Three major phenomena are identified for piston ring motion that affects blow-by, ring wear and oil consumption.

The term “ring lift” is given to the secondary axial motion of a piston ring, when it looses its contact with the ring groove under the action of mainly gas and inertia forces. The flow of gases past the piston ring is known to increase greatly during ring lift, compared to the sustained flow through the ring end gap. This is due to the large difference in flow area between large circumferential passage in case of ring lift and small ring end gap.

A phenomenon called “ring flutter”, often observed at high speed, low load conditions, has also been identified as the unstable relative movement of the piston ring in its groove. Due to low load, moderate pressure build up in the ring land above the ring causes a relatively lower gas force pushing the ring down. As a result, high inertial forces at high engine speed can lift the ring to the top side of the groove. The mechanism is not self correcting since the sealing at the bottom is lost which results in a high gas penetration and a lower pressure build up at increasing combustion gas pressure, causing

the instability. The forces acting at the ring top and bottom sides push the ring down and inertia forces push it back up again. This cycle is repeated many times resulting in increased blow-by and oil consumption.

“Ring collapse” is also an important situation which dramatically increases blow-by and oil consumption when occurred. This phenomenon is characterized as the loss of contact between the compression ring and liner, giving a flow path to combustion gases. The increase in blow-by is even greater than ring flutter in case of ring collapse, as there is more area and less resistance to pass in the circumferential opening than the clearance in the ring groove.

The first published analytical study to establish a comprehensive model coupling piston ring motion, land pressures and oil film was made by **Dursunkaya et.al. (1993)** with Ricardo RINGPACK code. They investigated the pressure situations in ring lands for a large diesel engine with four compression and one oil control ring. Their predictions show good correlation with experimental data obtained by pressure transducers in the ring lands.

An integrated and comprehensive study on ring dynamics and its effects on oil consumption has been made by **Herbst and Priebsch (2000)**. They used the AVL Glide which is also used analytical investigations during this study, to couple piston secondary dynamics, ring axial motion and lubrication theory to simulate and understand the effect of pressure balancing on oil consumption for a six-cylinder diesel engine oil consumption. Unlike the previously published gas flow models, which are based on the assumption that piston top land pressure is equal to the combustion pressure, they used an additional orifice at the top land. They also considered the difference in land pressures in piston major and minor thrust sides (thrust and anti-thrust sides) due to piston secondary motion. **Figure 2.8** shows the difference in clearance in major and minor thrust sides due to piston lateral motion. They reported that the secondary piston movement causes a choked gas flow on piston minor side during the compression stroke, and leads to an asymmetrical gas load. As a result, a lower amount of combustion gas discharges into the second ring land and causes a secondary ring fluttering.

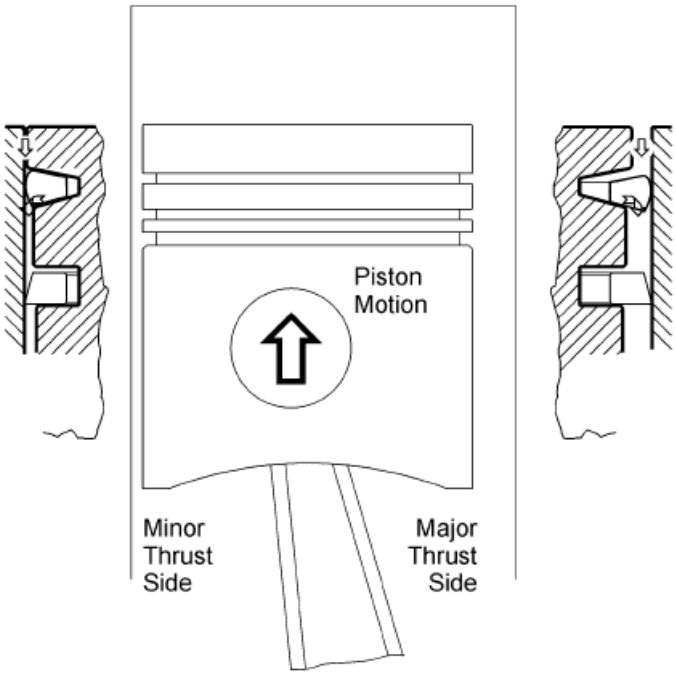

Figure 2.8: Piston Lateral Motion and Clearance **(Herbst and Priebsch, 2000)**.

Herbst and Priebsch achieved good correlation between predicted and measured land pressures by adjusting the flow parameters in their gas flow model so as to match measured total average blow-by with model predictions. They have shown that top edge scraping of the first compression ring can be influenced by second land pressure. In addition, top side sealing of the second ring and consequent increase in second land pressure may result in drastic decrement in face load of second compression ring. This occurs due to the tapered profile, causes the radial collapse of the second ring and leads to higher amount of oil remaining on the liner. Furthermore, the magnitude of inter-ring gas pressure is shown to be significantly different in major and minor thrust sides and this is attributed to the secondary movement of the piston.

3. THEORY OF AVL GLIDE - PISTON DYNAMICS, RING DYNAMICS AND OIL CONSUMPTION CALCULATION

Healthy assessments and conclusions can only be made with deep understanding and enough knowledge about the used computer code. Therefore, this section is dedicated to general information about main principles, approaches and assumptions of AVL Glide.

The software consists of three modules, Module Piston Movement, Module Ring Movement and Module Lube Oil Consumption. These modules will be touched on separately in the same order.

3.1. Module Piston Movement

Module Piston Movement is a tool to determine "piston secondary motion" in reciprocating engines. The tilting and transverse motion of the piston are calculated in thrust, anti-thrust (major-minor) plane, considering forces due to gas load, inertia, friction and the elasticity of the piston structure, as well as considering constraints due to the deformed contour of the liner . Results of GLIDE - Module Piston Movement help for optimization targets in piston and liner design, such as minimization of piston slap induced noise, cavitation and wear. It also provides input for engine block structure forced vibration analysis, however, in the context of this thesis, primary outcome of piston dynamic results are piston tilting and radial movement which are used in piston ring dynamics calculations by Module Piston Ring Dynamics.

3.1.1. General assumptions in piston dynamics calculation

The following assumptions are made in order to simplify the model in piston dynamics calculation **(AVL Glide User's Manual, 2005a):**

1. Calculation is only carried out for thrust (TS) and anti-thrust sides (ATS), ignoring circumferential effects.

2. Crankshaft angular velocity is assumed to be constant (Torsional vibrations and speed irregularities ignored).
3. Piston is considered to be elastic only in radial direction.
4. Liner, conrod and crankshaft are considered as rigid bodies.
5. Piston to liner damping is modeled empirically varying with deformation velocity.
6. Friction forces are considered according to friction functions without consideration of Reynold's equation.

3.1.2. Governing equations of piston dynamics

Figure 3.1 gives an overview of elements and geometric relations involved in piston dynamics calculation and provides the negative/positive sense for the generalized coordinates. When piston stiffness is ignored the mechanism has three degrees of freedom (designated with generalized coordinates x_p, y_p and κ) different from the single-degree-of-freedom slider crank mechanism.

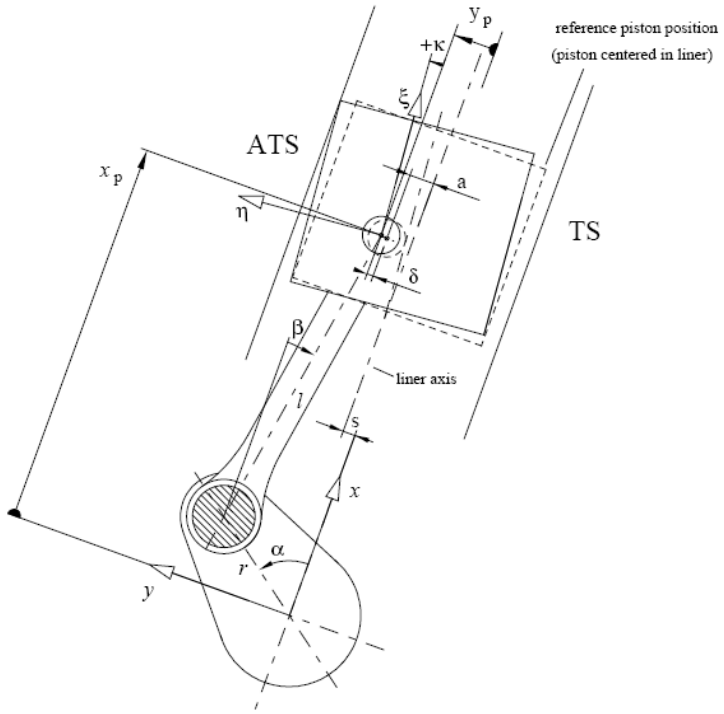

Figure 3.1: Cranktrain Reference Frame and Definition of Piston Movement

The free-body diagram of piston is shown below in **Figure 3.2.**

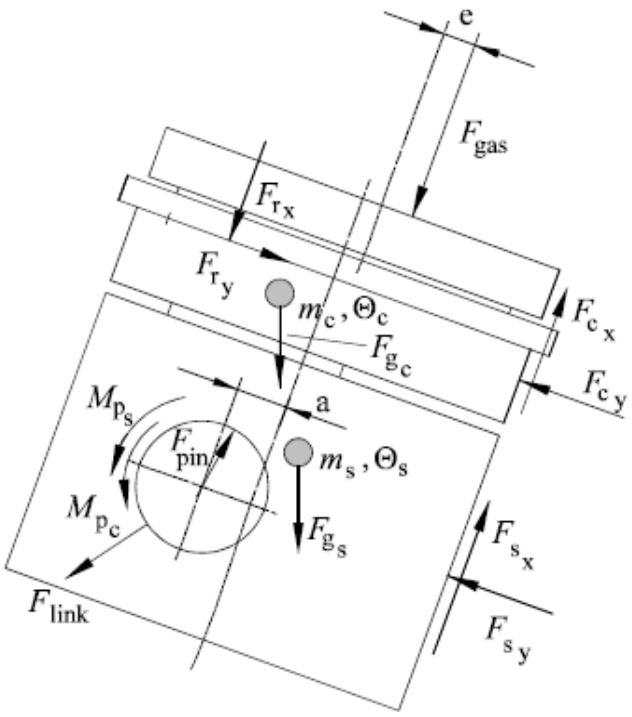

Figure 3.2: Free-Body Diagram of Piston

From the free body diagram, direct application of Newton's second law of motion yields the following equations:

x-direction:

$$m_p \cdot \ddot{x} = \sum F_x = \sum F_{cx,i} - F_{gx} - F_{gas} - F_{rx} + F_{pinx} \quad \textbf{(3.1)}$$

y-direction:

$$m_p \cdot \ddot{y} = \sum F_y = \sum F_{cy,i} - F_{gy} - F_{ry} + F_{piny} \quad \textbf{(3.2)}$$

Dynamic moment equilibrium around pin center:

$$I_p \cdot \ddot{\kappa} = \sum M = \sum M_{ci} + M_g + M_{gas} + M_r + M_p \quad \textbf{(3.3)}$$

The forces F_{link} from the links connected to the piston pin are omitted since there are not any links attached to the pin.

The above symbols refer to following quantities:

m_p : Piston mass

I_p : Piston moment of inertia around pin center

F_g : Weight of piston

F_{gas} : Force due to combustion pressure

F_r : Piston ring contact force

F_{ci} : Liner contact force at thrust and anti-thrust sides at i'th cross section

F_{pin} : Force exerted by piston pin on piston

M_{ci} : Moment due to piston-liner contact at i'th cross section

M_g : Moment due to piston weight

M_{gas} : Moment due to gas force (active when the combustion chamber is non-symmetric)

M_r : Moment due to ring axial and radial contact force

M_p : Moment due to friction at piston pin

$\ddot{\kappa}$: Angular acceleration of piston

The forces acting on the piston pin are further calculated from dynamics of connecting rod. The free-body diagram of the connecting rod is given in **Figure 3.3.**

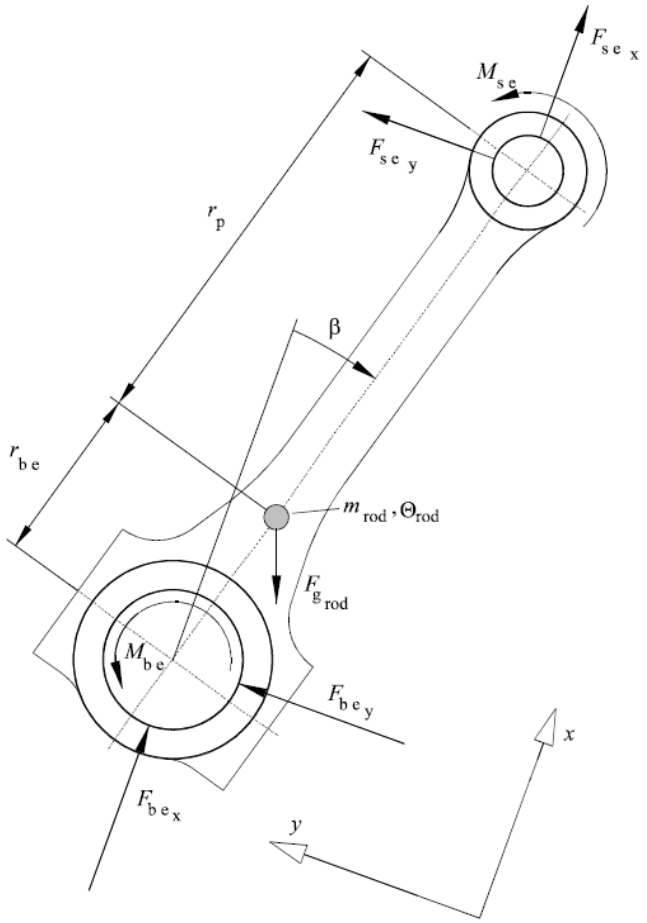

Figure 3.3: Free Body Diagram of Connecting Rod

Again direct application of Newton's second law of motion yields:

In x-direction:

$$m_{rod} \cdot \ddot{x}_{rod} = \sum F_x = \sum F_{sex} + F_{bex} - F_{grodx} \qquad \textbf{(3.4)}$$

In y-direction:

$$m_{rod} \cdot \ddot{y}_{rod} = \sum F_x = \sum F_{sey} + F_{bey} - F_{grody} \qquad \textbf{(3.5)}$$

In addition, dynamic moment equilibrium around mass center yields:

$$I_{rod} \cdot \ddot{\beta} = \sum M = M_p + M_{be} + F_{sex} \cdot r_{py} - F_{sey} \cdot r_{px} + F_{bex} \cdot r_{bey} - F_{bey} \cdot r_{bex} \qquad \textbf{(3.6)}$$

Where:

m_{rod} : Conrod mass

I_{rod} : Conrod moment of inertia around center of mass

F_{se} : Force at conrod small end bearing

F_{be} : Force at conrod big-end

F_{grod} : Weight of conrod

M_{se} : Moment due to friction at small-end bearing

M_{be} : Moment due to friction at big-end bearing

r_p : Conrod center of mass to small-end bearing center distance

r_{be} : Conrod center of mass to big-end bearing center distance

The piston motion itself is calculated in time domain by means of integration methods. A constant width is used for the time step. A pre-calculation of 60 DEG CA is used to determine initial conditions for the movement of the piston at 90 DEG CA before TDC.

The initial conditions for pre-calculation are zero-velocities and zero-accelerations. Starting at 90 DEG CA before TDC one engine cycle will be calculated. The equilibrium of elastic forces between piston and liner and in the pin bearing (equilibrium between piston and conrod) has to be determined iteratively using NEWTON-RAPHSON method. **Figure 3.4** provides an overview of the scheme of calculation.

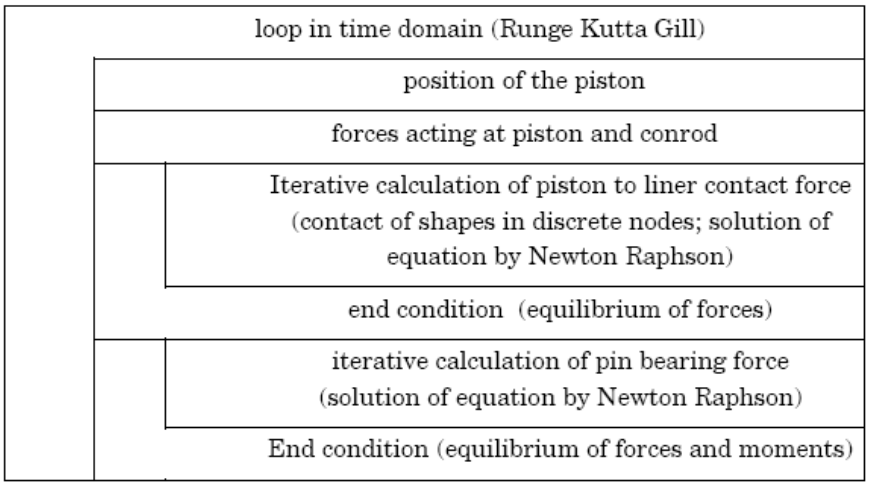

Figure 3.4: Piston Movement Computation Scheme

3.2. Module Piston Ring Movement

AVL GLIDE - Module Piston Ring Dynamics was developed in order to be able to analyze effects of design modifications of piston and piston rings in view of low LOC, blow-by and friction values. For the determination of the dynamic loads upon the rings, GLIDE -Module Piston Ring Dynamics considers forces and moments due to inertia, friction and the flow of gas from the combustion chamber through the inter-ring volumes into the sump. If the influence of piston slap on ring dynamics should be taken into account, the program uses the results from piston slap calculation as input, which is pre-calculated for either a mono piston or an articulated piston (GLIDE - Module Piston Movement**)**. From these results, ring dynamics are influenced by both the piston radial and tilting motions.

The results of the Piston Ring Dynamics Calculation show the dynamic components of motion of the single rings in a thrust - anti-thrust plane. The simulation also gives values for blow-by, inter-ring pressures and oil film thickness between the rings and liner over crank angle.

The main characteristics of the Software GLIDE - Module Piston Ring Dynamics can be listed as follows:

1. Each ring is modeled as a single mass. The interaction between the thrust and anti-thrust sides is given by a beam model and a model for pressure compensation. Twisting (including pre-twist angle) is considered.
2. For the calculation of the gas flow through the rings, inter-ring regions are considered as volumes, which are given by the piston and ring geometries and the actual clearances between piston and liner. The volumes are connected due to the actual clearances of ring end gaps and actual position of the rings in the grooves.
3. The possible gas flow behind the rings and between ring and groove flanks is considered. The oil film is taken into account between the ring running surface and liner by calculating the pressure distribution in the clearance according to the liner and ring contours.

3.2.1. General assumptions in piston ring dynamics calculation

The following assumptions are made for calculation of piston ring dynamics **(AVL Glide User's Manual, 2005b)**:

1. The calculation is simultaneously done at TS (thrust side) and ATS (anti thrust side), the mutual influence being taken into account ("quasi three-dimensional") by the consideration of gas flow through the ring groove and geometric considerations. Along the circumference, constant conditions are assumed.
2. Rings are approached as single masses.
3. The radial mass forces of the rings are neglected
4. The equation of motion in radial direction is not solved explicitly; there will only be a calculation as to whether the ring is lifted from the liner wall.
5. The radial friction force between ring flanks and piston ring groove is calculated by means of the Friction Function according to Stribeck.
6. The calculation of the gas flow and pressure is quasi stationary (constant conditions in each time step) being done by a system of chambers and throttling points. Flow processes are considered as being isothermal. The max. velocity of flow is limited to the sound velocity at the throttling points.
7. There won't be any pressure drop in the piston top land, the combustion pressure acts above the top ring. Below and behind the oil ring, the crankcase pressure is active.
8. The gas pressure distribution in the flank clearance between ring and groove is calculated by assuming the pressure gradient as being indirectly proportional to the current clearance.

3.2.2. Governing equations of ring dynamics

The forces acting on a piston ring were shown in **Section 2.3**. The figure is repeated here for easy following **(Figure 3.5).**

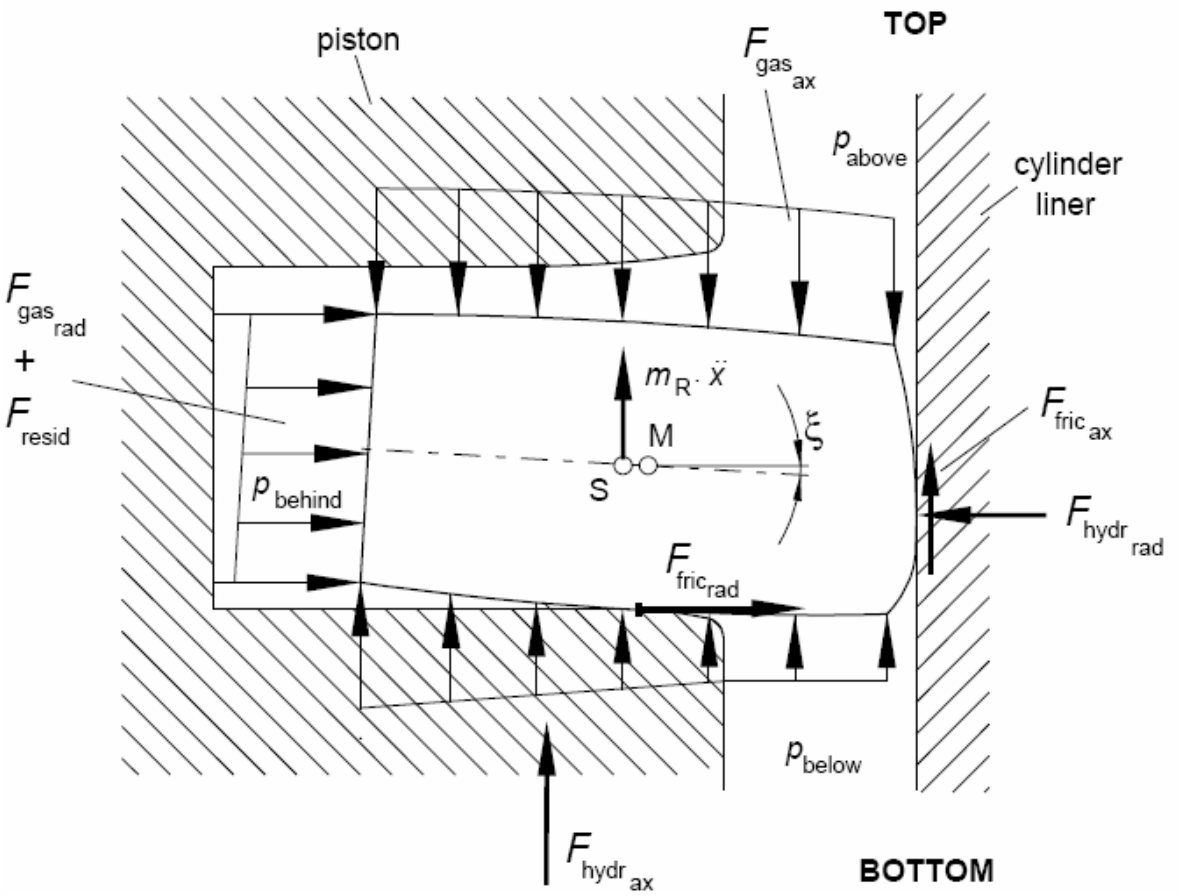

Figure 3.5: Forces Acting on Piston Ring **(AVL Glide User's Manual, 2005)**

In axial direction:

In order to judge whether the ring is in contact with the groove flank, contact force between the ring and groove is calculated as:

$$F_{contact,ax} = F_{inertia,ax} + F_{fric,ax} + F_{gas,ax} + F_{bend} \quad \textbf{(3.7)}$$

If $F_{contact,ax} > 0 \Rightarrow$ There is contact with the piston and ring does the same motion as the piston, i.e.:

$$x_{ring} = x_{piston} \quad \textbf{(3.8)}$$

If $F_{contact,ax} > 0 \Rightarrow$ The ring lifts from groove flank, hence the dynamics equation has to be solved:

$$m_{ring} \cdot \ddot{x}_{ring} = \sum F = F_{fric,ax} + F_{gas,ax} + F_{hydr,ax} + F_{bend} \quad \textbf{(3.9)}$$

Where the symbols refer to the following:

m_r : Mass of piston ring

$F_{fric,ax}$: Axial friction force between liner and ring surface

$F_{gas,ax}$: Axial gas force

$F_{hydr,ax}$: Damping caused by the oil filling of the groove

F_{bend} : Bending force caused by the interaction between TS and ATS

In radial direction:

The contact force between the ring and liner is calculated as:

$$F_{contact,rad} = F_{gas,rad} + F_{tension} + F_{fric,rad} \quad \textbf{(3.10)}$$

If $F_{contact,rad} \leq 0 \Rightarrow$ ring lifts from the liner. In this case the equation of motion is not solved explicitly.

Where the symbols refer to:

$F_{tension}$: Force caused by the tension of the ring

$F_{gas,rad}$: Gas force

$F_{fric,rad}$: Friction force between ring and ring groove

$F_{hydr,rad}$: Force caused by the hydrodynamic gap between liner and ring running surface (including radial damping force)

3.2.3. Twisting of the piston ring

Moment equilibrium around the center of cross section (Point M in **Figure 3.5**):

$$\sum M = \sum (F_i \cdot h_i) + M_{pre-twist} = M_{elastic} \cdot \xi \quad \textbf{(3.11)}$$

Where the symbols refer to:

$M_{elastic}$: Elastic bending moment against ring twisting

$M_{pre-twist}$: Elastic moment due to pre-twist angle

h_i : Moment arm for each force component

3.2.4. Gas flow through the ring pack

One of the main challenging points in ring dynamics is that ring dynamics and gas dynamics in the ring pack depend on each other. Since inertial forces and gas forces are the main drivers of ring motion, healthy evaluation of gas forces is essential.

For the calculation of gas forces acting upon rings, the pressure resulting from the gas flow have to be known. For this, the entire ring package will be divided into chambers (volumes behind and between the rings), which are connected one to another by throttling points (see **Figure 3.6**).

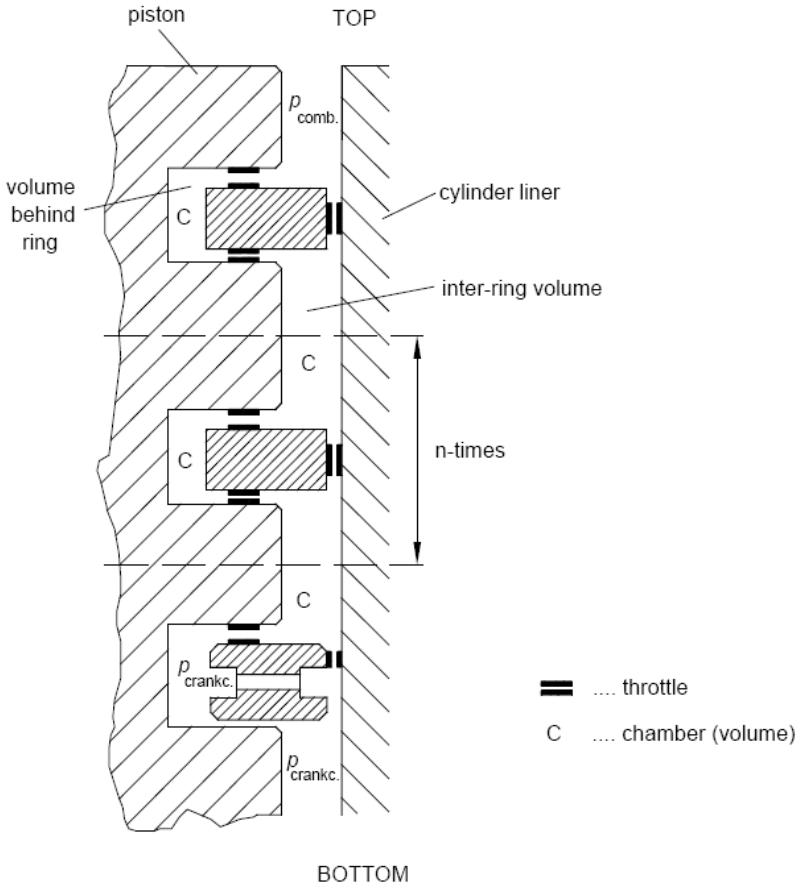

Figure 3.6: Gas Flow Model for Entire Ring Package

Starting upon the known pressure p_{comb} on the piston top land and p_{crankc} below or behind the oil ring, the pressures in the chambers will be determined in a quasi stationary way by means of a step-by-step calculation of the gas masses flowing through the throttling points.

The basic model used is the flow process from a chamber with the state quantities p_C, T_C, V_C into the surroundings or from a different chamber with the state quantities p_o, T_o, V_o via a throttle with cross sectional area A and gas flow coefficient ψ (see **Figure 3.7**):

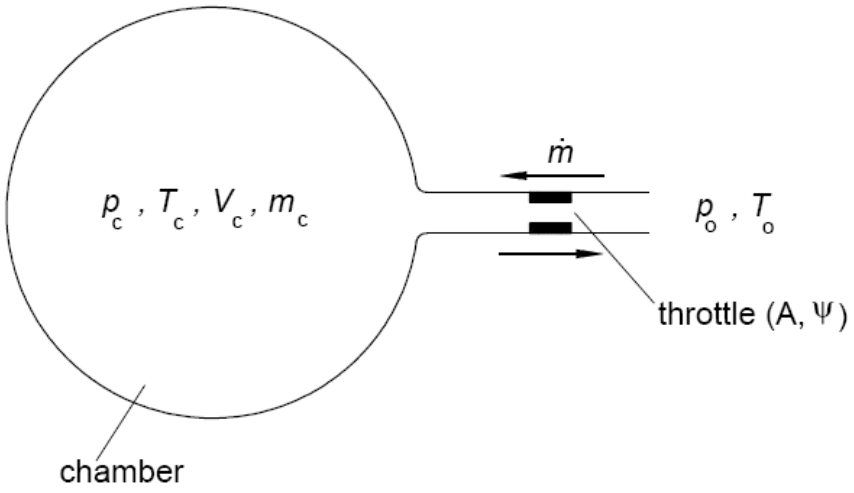

Figure 3.7: Gas Exchange Process from a Chamber

Two important considerations for the flow process are that isothermal change in the state is assumed and max. gas velocity is limited by the speed of sound in the throttle.

Mass flow:
$$\dot{m} = A \cdot \psi \cdot p_c \cdot \sqrt{\frac{2}{R \cdot T_c}} \cdot \sqrt{\frac{k}{k-1} \cdot \left[\left(\frac{p_0}{p_c} \right)^{\frac{2}{\kappa}} - \left(\frac{p_0}{p_c} \right)^{\frac{k+1}{k}} \right]} \quad \textbf{(3.12)}$$

Rate of change of mass:
$$\Delta m = \dot{m} \cdot \Delta t \quad \textbf{(3.13)}$$

Pressure in the chamber:
$$p_c = \frac{R \cdot T_c}{V_c} \cdot (m + \Delta m) \quad \textbf{(3.14)}$$

Where the symbols refer to:

R : Gas constant of combustion gas

k : Isentropic exponent

Δt : Time step

For the gas flow, the following throttling points are considered:

- Ring running surface (see **Figure 3.8**) including end gap (see **Figure 3.9**)
- Ring flanks (top and bottom side) (see **Figure 3.8**)

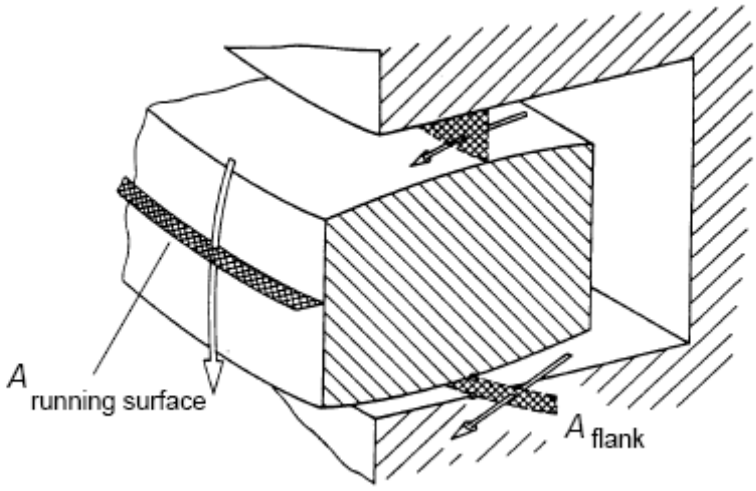

Figure 3.8: Throttling Points and Discharge Areas at Ring Flanks

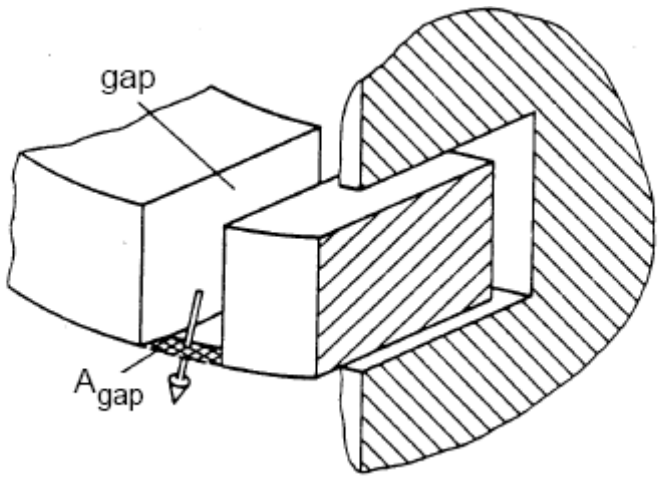

Figure 3.9: Throttling Point and Discharge Area at End Gap

The gas flow at ring running surface and flanks is calculated by considering gap areas caused by the current position of the ring relative to the groove and due to ring surface roughness (microscopic flow areas).

3.2.5. Hydrodynamic and asperity contact at ring face

The gap between the piston ring running surface and the cylinder wall is considered as being a hydrodynamic slider of infinite length in circumferential direction. Adopting the usual assumptions of hydrodynamic lubrication theory for rough bearing surfaces the governing Reynolds equation for pressure generation in the fluid film taking an isoviscous, incompressible lubricant states **(Patir and Cheng, 1979)**:

$$\frac{\partial}{\partial x}(\Phi_x h^3 \frac{\partial \overline{p}}{\partial x}) = 6\eta U\sigma \frac{\partial \Phi_s}{\partial x} + 12\eta \frac{\partial \overline{h}_T}{\partial t} \qquad \textbf{(3.13)}$$

Where:

h : Nominal film thickness

$\overline{h}_T$: The average gap

$\overline{p}$: Mean hydrodynamic pressure

σ : Composite surface roughness

Φ_x : Pressure flow factor

Φ_s : Shear flow factor

U : Sliding velocity

The cavitation boundary condition is taken as:

$$\overline{p} = \{p = pCav : dp/dx = 0 \qquad \textbf{(3.14)}$$

It is evident that compression rings operate nearly always in starved conditions. That means the gap between the ring face and cylinder wall is not completely filled or flooded with lubricant. The supply with oil is individually determined for each ring using the so-called Filling Percentage (FP) as described in the following figure (see **Figure 3.10**):

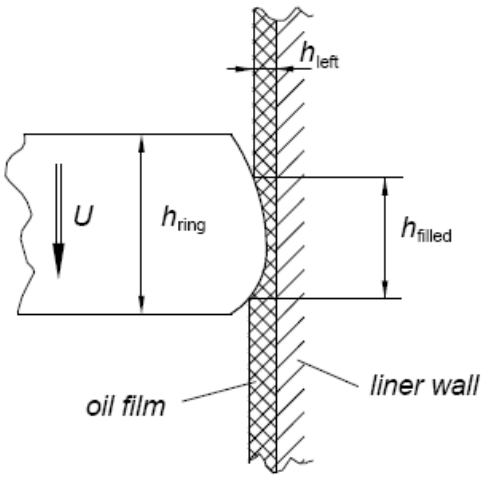

Figure 3.10: Filling Percentage

In order to consider the oil filling percentage, one ring will only get so much oil as this corresponds to the oil film left on the liner wall by the previous ring. As for the downstroke of the oil ring, complete filling (*FP*=100%) is assumed due to the splashed oil on the liner. The definition of oil filling percentage is as follows:

$$FP = \frac{h_{filled}}{h_{ring}} \tag{3.15}$$

The filling percentages will be acquired iteratively within the hydrodynamic calculation. The simultaneous calculation of the oil film thickness and the oil flow at the entire ring package leads to realistic oil film distributions along the liner wall, which are very important for the prediction of lube oil consumption and friction estimations.

3.2.6. Asperity Contact Model

In the mixed lubrication regime the model according to **Greenwood and Tripp (1971)** is applied for asperity interaction of two rough surfaces.

3.2.7. Interaction between thrust and anti-thrust sides

The interaction between the two calculation sides is handled by the following models.

If the ring is lifted on one side, this will result in an elastic reaction force (bending force) F_{bend}, which wants to move the ring back (**Figure 3.11**):

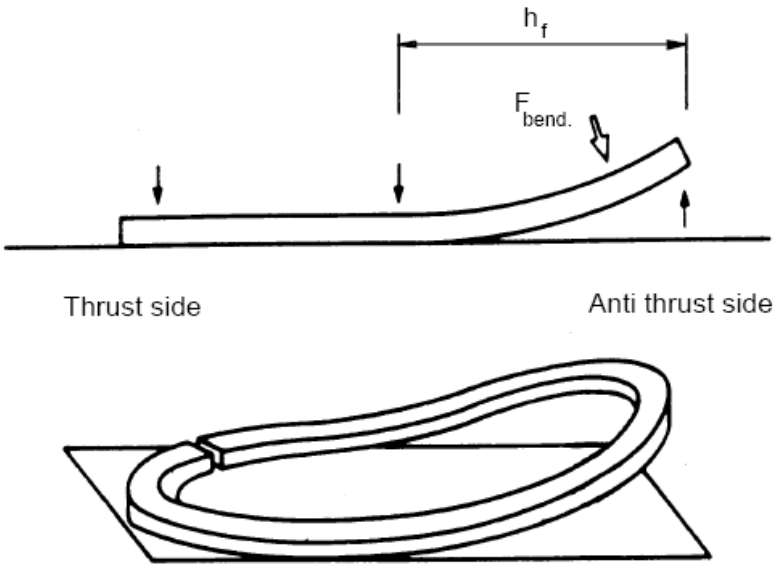

Figure 3.11: Elastic Coupling Model for Thrust and Anti-Thrust Side Interaction

For pressure compensation between thrust and anti-thrust sides, the following model is used (**Figure 3.12**):

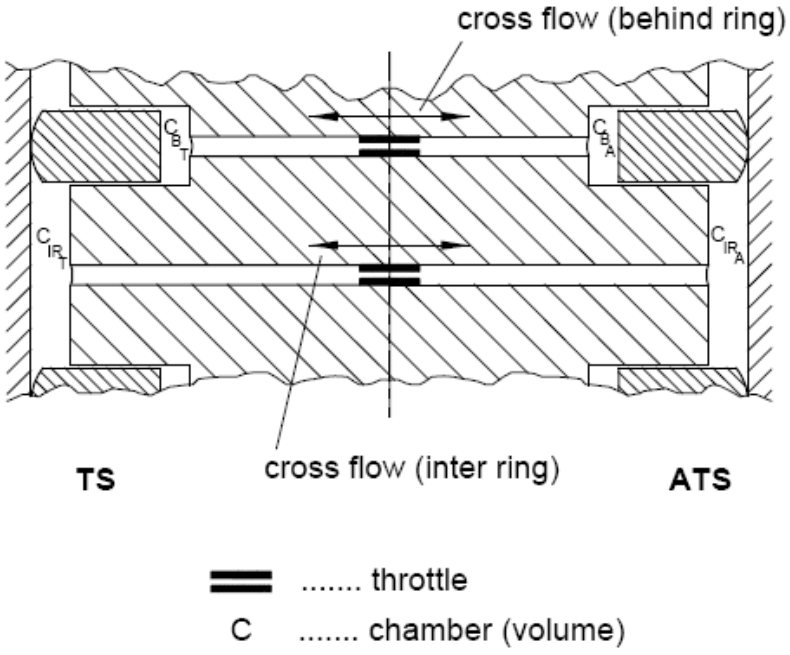

Figure 3.12: Cross Flow between Thrust and Anti-Thrust Sides through the Ring Groove

3.3. Module Lube Oil Consumption

The following oil consumption sources are considered in Module – Lube Oil Consumption:

1. Evaporation of lube oil from liner wall
2. Oil throw-off of accumulated oil (e.g. due to ring scraping) above the top ring due to inertia forces.
3. Oil blow through the end gap of the top ring into the combustion chamber due to a negative pressure gradient (pressure at 1st inter ring volume greater than combustion pressure)
4. Oil scraping at piston top land's edge (considering deposits at top land)

3.3.1. Evaporation from Liner Wall

The evaporation of lube oil from the cylinder liner wall is simulated by a diffusion process in a medium with flow velocity **(see Figure 3.13)**

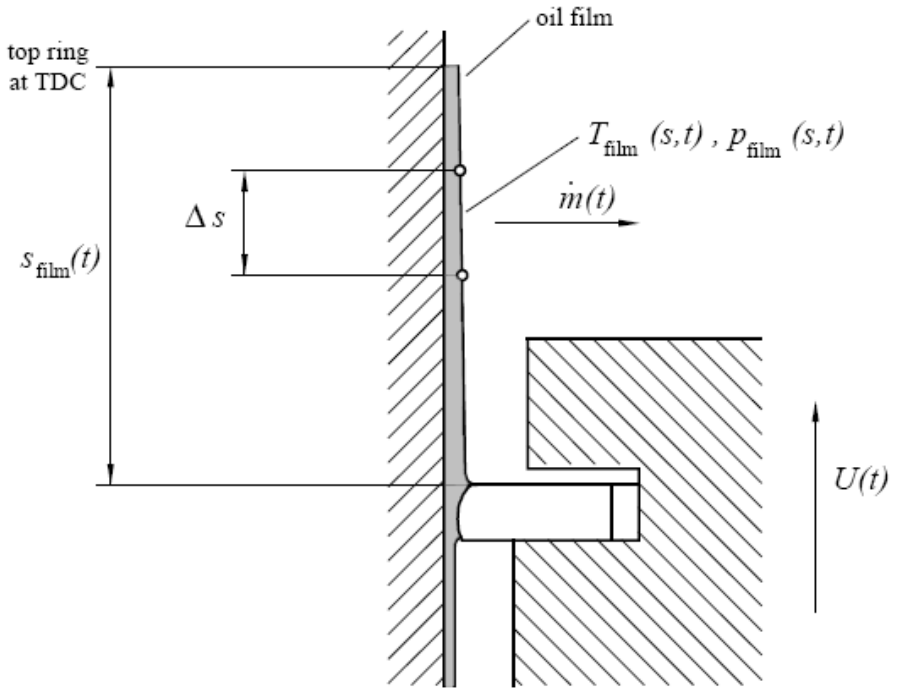

Figure 3.13: Oil Mass Flux into Combustion Gas

The stationary convective material-exchange between two media (especially between lube oil and combustion gas) is described by the following equation:

$$\beta \cdot (c_{film} - c_{\infty}) = \dot{m} = -D \cdot \frac{dc}{dy} \qquad \textbf{(3.16)}$$

Where:

β : Mass transfer coefficient

c_{film} : Concentration of lube oil at film surface

c_{∞} : Concentration of lube oil in combustion chamber

$\dot{m}$: Mass flow rate into boundary surface

y : Coordinate perpendicular to boundary surface

Δs : Movement of the piston during time step Δt

s_{film} : Uncovered area of the oil film

For the calculation of the temperature T_{film} of the oil film surface, an oil vapor layer (100% oil) above the oil film is assumed as shown in **Figure 3.14**:

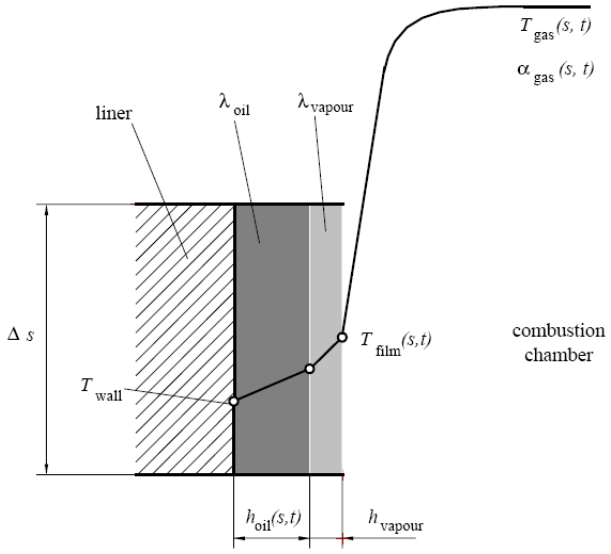

Figure 3.14: Temperature Distribution from Liner Wall to Combustion Gas

The thickness of the oil film h_{oil} is given by the piston ring dynamics calculation.

3.3.2. Oil throw-off from top compression ring

The flow balance of lube oil over the first piston ring and the consideration of the piston acceleration enable the calculation of the thrown-off oil quantity. The possible thrown-off oil quantity is determined by the current oil volume above the top ring (between piston top land and liner wall) and the acceleration of the piston. The following transport mechanisms lead to a decreasing or increasing of the accumulated oil at the top side of the first ring.

3.3.2.1. Oil transport mechanisms onto top ring

1. The oil scraping of top ring - Calculated by the difference in left oil film thickness during the upwards and the downwards motion of the top ring
2. Oil flow through the ring gap into the second land (decreasing the accumulated oil) - Due to positive pressure gradient (combustion pressure greater than 1st interring pressure) oil accumulated above the first ring will flow down the gap into the 2nd land. The oil flow due to a negative pressure gradient into the combustion chamber is assumed as instantaneous loss of the oil.
3. Oil flow through the ring groove - The oil flow from the area behind the ring to the area above the ring is caused by the squeezed oil, if the ring moves relative to the piston (axial "pumping" of the ring) and by the flow due to the pressure gradient as shown in **Figure 3.15.**

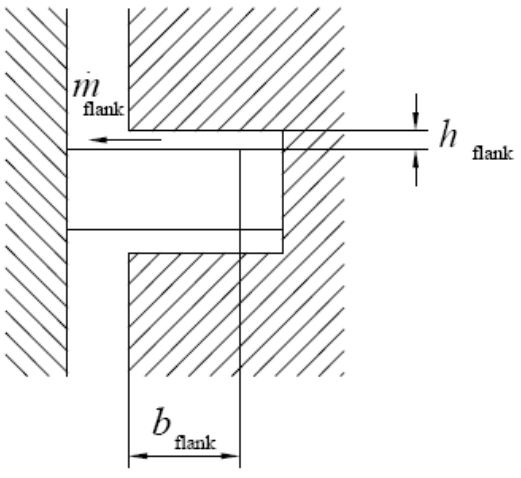

Figure 3.15: Oil Transport through Ring Groove

3.3.2.2. Calculation of thrown-off volume

For the simulation of the thrown-off quantity of the accumulated oil between the piston top land and the liner wall, the entire film is divided into discrete layers. Within these layers a constant acceleration is assumed. Between the layers the shear stress according to Newton is acting. Oil is considered to be transported to the combustion chamber and consumed if inertial forces acting on the ring overcome shear forces as shown in **Figure 3.16.**

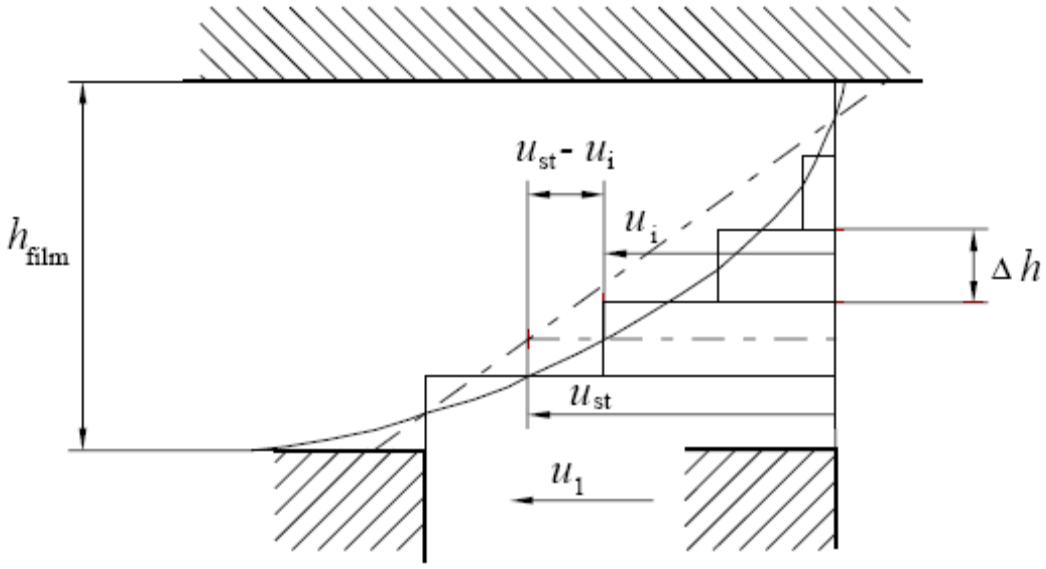

Figure 3.16: Velocity Distribution in Discrete Layers of Oil Film

Finally, the thrown-off oil volume can be calculated as follows:

$$V_{throw-off} = (u_m - u_{st,m}) \cdot h_{film} \cdot d_{film} \cdot \pi \cdot \Delta t \quad \textbf{(3.17)}$$

Where the symbols refer to:

$$u_m = \frac{\sum u_i}{i} \quad \textbf{(3.18)}$$

$$u_{st,m} = \frac{a_0 \cdot \Delta t}{2} \quad \textbf{(3.19)}$$

a_0 : Acceleration at the beginning of motion

h_{film} : Height of oil film between top land and liner

d_{film} : Diameter of oil film

3.3.3. Oil Blow through top ring end gap

The pressure gradient over the top ring allows computing the oil blow through the end gap into the combustion chamber. In case of a negative pressure gradient over the top ring (combustion pressure less than pressure at 2nd land) oil is blown through the end gap. The oil quantity due this effect is assumed as an instantaneous oil loss and is not exposed the inertia forces.

3.3.4. Top land scraping

The scraped amount of oil is calculated by considering the piston's lateral movement and tilting motion together with geometric conditions **(Figure 3.17).**

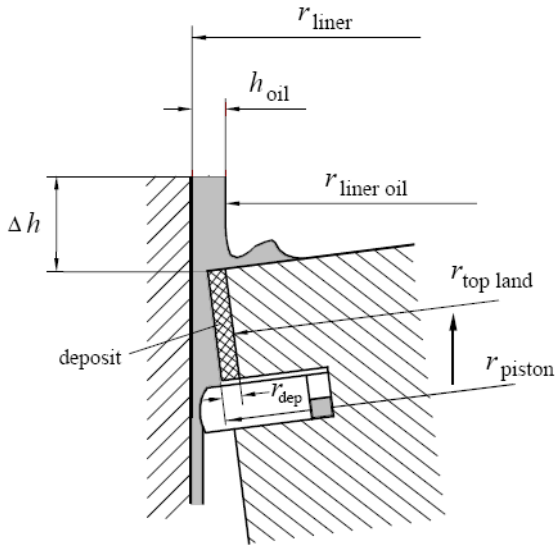

Figure 3.17: Top Land Scraping Geometric Considerations

4. PISTON DYNAMICS, RING DYNAMICS AND OIL CONSUMPTION MODEL FOR ECOTORQ 9.0 L ENGINE

A piston dynamics, ring dynamics and oil consumption model for FORD ECOTORQ 9.0 L engine is established using AVL Glide simulation code. The model consists of the piston, piston pin, liner, conrod, and piston rings as shown in **Figure 4.1.**

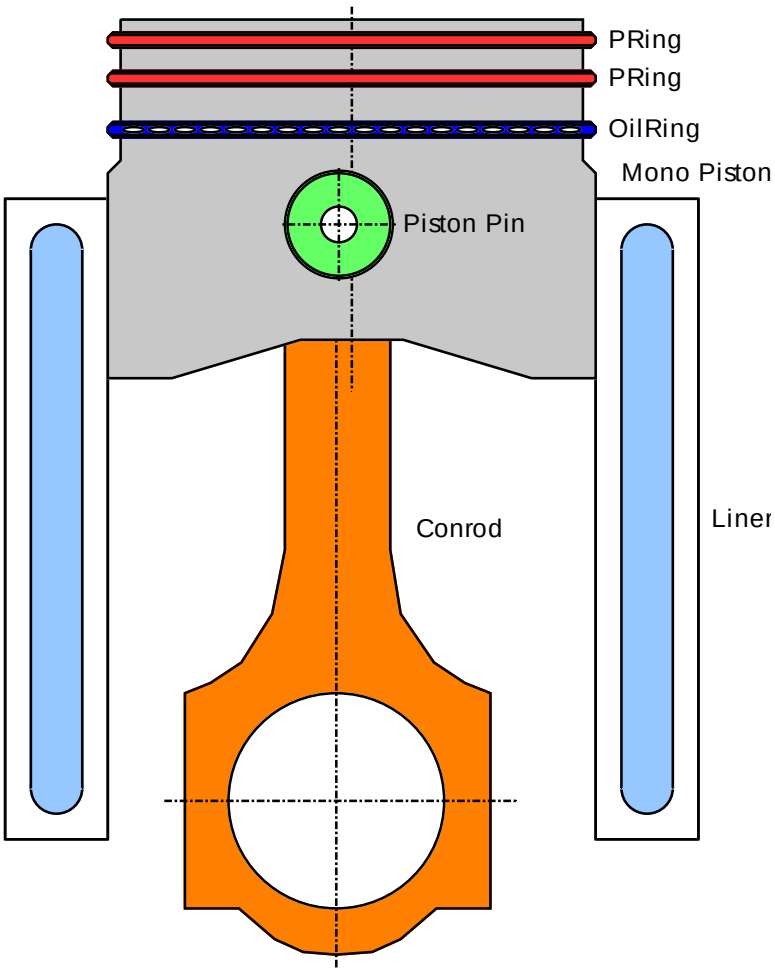

Figure 4.1: Piston Assembly Model

The general specifications of the engine under investigation are given **Table 4.1.**

Table 4.1: General Specifications of Ecotorq 9.0 L Engine

Engine configuration:	6 Cylinder in-line
Fuel injection system:	(1800 bar) Common Rail DI Diesel
Scavenging system:	Turbo-charged, inter-cooled
Bore:	115 mm
Stroke:	144 mm
Swept volume:	8.974 L
Rated power:	295 kW at 2200 rpm
Peak torque:	1600 Nm at 1200 rpm
Max. Operational speed:	2200 rpm
Max. continuous overspeed:	3100 rpm
Valve train:	OHV, 4 valves per cylinder

4.1. Piston, Liner and Cranktrain

The geometrical data for the piston and liner in cold state are used for the simulation since data is not available for the hot profiles. Therefore, the piston-to-liner clearances are larger than actual operating conditions in the model. Furthermore, the deformation of the liner due to cylinder head bolt clamp loads is also ignored. The data of the piston and liner are given in **Appendix 1.1.**

The stiffness matrix of the piston is extracted by using the CAD model of the piston and finite element solver Abaqus. First, the flexibility matrix of the piston is determined by finite element method, and than Glide obtains the stiffness matrix by matrix inversion. The inertial properties of the piston pin are also included in piston properties.

4.2. Piston Rings and Ring Groove

The geometrical data of the piston rings as well as estimations for their operating temperatures are used for the calculation. Therefore, the hot geometry of the rings and groove are calculated according to thermal expansion considerations. The data used for piston rings are summarized in **Appendix 1.2.**

The flow factors that are used in the calculation for gas flow between ring lands and ring grooves are very important for inter-ring pressures and ring dynamics calculations. A

comparison of initially calculated blow-by values with typical blow-by values of the engine show large differences, when default flow factor suggested by the program are employed. Although these flow factors are based on correlation with measured data, the difference between engines in many aspects causes this gap in blow-by. Therefore, the flow factors are decreased in order to better match with blow-by data. The flow factor for the upper groove of the first ring is assigned a relatively higher value because of the keystone angle. The closed gap values of piston rings have also high importance in the calculations. Therefore, the ring gaps of the engine that will be under investigation during experimental studies have been measured prior to assembly and these data are used in the calculations.

5. OIL CONSUMPTION AND IN-CYLINDER PRESSURE MEASUREMENT

In this section, it is aimed to provide some general information on the measurement techniques used in this thesis. These are the lube oil consumption measurement using SO_2 (sulphur dioxide) tracing technique and in-cylinder pressure measurement using piezoelectric type pressure transducer and angle encoder working with fiber optical principal. However, it should be mentioned that the measurement techniques are not the focus of this study and they are only used to asses the analytical results. Therefore, only main principles of the methods are given to provide relevant background to evaluate the results of measurements.

5.1. Oil Consumption Measurement Using SO2 Tracing Technique

The working principle of the SO2-technique is to operate the engine on a lubricant and diesel with known sulfur concentrations. The engine oil consumption can thereby be back-calculated based on the sulfur-concentration measured in the engine exhaust. The quantities needed for oil consumption measurements are:

1. Air flow rate
2. Rate of fuel (diesel) consumption
3. SO_2 concentration in engine exhaust gas

The intake air flow rate and fuel flow rate are measured during engine operation by integrated equipment in the test bench and SO_2 concentration in the exhaust gas is measured using V&F Twin MS mass spectrometer shown in **Figure 5.1.**

Figure 5.1: V&F Twin MS

The V&F twin mass spectrometer works with IMF (Ion Molecule Reaction) principle. The ionized molecules are separated in the octopol separator focusing on primary ions and filtering out any interference. The quadrupol mass filter (0-500 amu) then separates the molecules for further detection at the fast pulse counter. These components and phases are shown in **Figure 5.2.** The technical specifications of the mass spectrometer are provided in **Appendix 2.1**

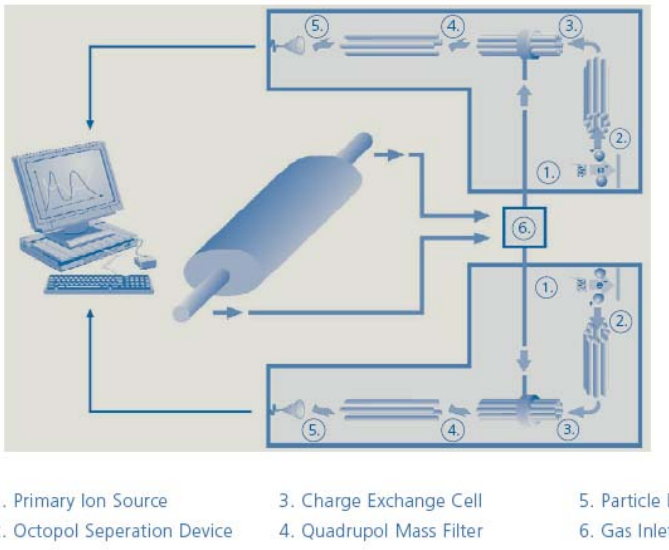

Figure 5.2: Main Components of Twin MS

After acquisition of data the oil consumption is calculated as follows **(Froelund, 1999)**:

$$\dot{m}_t^{oil} = \frac{\dot{m}_t^{fuel} \cdot ([S]_t^{Exh} - [S]_t^{Fuel}) + \dot{m}_t^{Air} \cdot ([S]_t^{Exh} - [S]_t^{Air})}{[S]_t^{Oil} - [S]_t^{Exh}} \quad \textbf{(5.1)}$$

Where the quantities are defined as follows:

$\dot{m}_t^{oil}$: Oil consumption at time t

$\dot{m}_t^{fuel}$: Fuel mass flow rate at time t

$\dot{m}_t^{Air}$: Air mass flow at time t

$[S]_t^{Oil}$: Sulfur concentration of oil

$[S]_t^{Fuel}$: Sulfur concentration of fuel at time t

$[S]_t^{Air}$: Sulfur concentration of air at time t

$[S]_t^{Exh}$: Sulfur concentration in exhaust gas at time t

For more information about SO_2 tracing technique see references **(Ariga, 1996, Ariga, 1992, Ariga et. al. 1992a, Ariga et. al. 1992b)**.

5.2. In-Cylinder Pressure Measurement

Measurement of cylinder pressure with sufficient accuracy also plays a key role in this study. In general, the difficulties in cylinder pressure measurement are high values of measured pressures (up to 190 bar), high temperature of combustion gas (~1300°C) and consequently pressure transducer (~300 °C) and very high speed of the signal.

The components of the in-cylinder measuring system are as follows:

1. AVL GU12P un-cooled piezosensor
2. AVL 365C angle encoder set
3. AVL Indiset 620 data acquisition system and software

The cylinder pressure signal is obtained from the first cylinder of the engine by mounting the piezosensor between the intake valves of the first cylinder. The technical

specifications of GU12P un-cooled piezosensor is given in **Appendix 2.2**. Since the piezo-electric type pressure transducers measure with reference to a known pressure, the pressure at 180° crank angle is taken as reference. The cylinder pressure at this point is assumed to be equal to boost pressure, so the measured boost pressure is added to the measured cylinder pressure for correction.

AVL 365C angle encoder carries out crank angle determination by means of a fiber optical pick-up which is mounted at the front-end of the crankshaft with an intermediate flange. Since this is an optical measurement technique and all electrical components are in direct contact with the engine, they are neither exposed to mechanical stress nor high component temperatures.

AVL Indiset 620 enables the acquisition, conditioning and storage of pressure data. The software enables the synchronization of angle and pressure signals and TDC (Top Dead Center) determination by using the fact that during motoring conditions the highest cylinder pressure occurs at TDC.

6. ANALYSIS OF EFFECT OF PFP ON DIESEL ENGINE OIL CONSUMPTION

The decision on the operating peak firing pressure of a diesel engine is one of the most critical issues in development of a diesel engine. Since the fuel economy (brake specific fuel consumption) and exhaust emissions, both in terms of nitrous oxides and particulates, strongly depend on distribution of the combustion pressure within the cycle, as it is one of the main thermodynamic indicators of the combustion quality within the cylinder where the other is the temperature. In addition to emissions, the maximum pressure is also constrained by structural considerations because the power cylinder components carry the loads induced by the combustion pressure some billion cycles, hence the load amplitudes are directly proportional to peak pressures in fatigue considerations.

While it is a well known fact that peak firing pressure of an engine is subject to a challenging optimization under objective mentioned above, generally oil consumption is not taken into evaluation in this optimization. This study aims to point out and quantify the influence of combustion pressure mainly on oil consumption and also on blow-by. Although focus is placed on oil consumption, blow-by is also investigated at one side since it is easily monitored in real time, the two are strongly inter-related and blow-by trends provide a deeper understanding of mechanisms behind oil consumption.

The shape of the combustion pressure is characterized in general by two parameters, namely the indicated mean effective pressure (IMEP) which is the average value of the curve, and the peak firing pressure which is the maximum value on the curve. When the representative pressure value for total friction in the engine (friction mean effective pressure or FMEP) is subtracted from IMEP, brake mean effective pressure is obtained. BMEP is considered to be the main indicator of load or torque, in order to indicate a particular operating point, together with engine speed. When the peak value of cylinder pressure is increased, the skirt of the curve becomes steeper to compensate the

difference in enclosed area. As a result, rings and piston experience higher pressure close to TDC, while pressure drops faster through the exhaust stroke.

In this section, the effect of peak firing pressure on oil consumption and blow-by characteristics of Ecotorq 9.0 L diesel engine is investigated for two operating points, the maximum power (2200 rpm, 1270 Nm) and maximum torque (2200 rpm, 1270 Nm) points. Maximum power point is selected because it demonstrates the behavior of power cylinder at highest speed, where engine is able to provide torque and therefore oil transport mechanisms are very active. The oil consumption is also highest at this point which makes optimization for oil consumption feasible. The maximum torque point is selected because the oil consumption behavior at this point is especially crucial as it has high contribution in total duty cycle of heavy duty engines.

6.1. Analytical Investigations

6.1.1. 1600 rpm, full load operating point

Two simulations have been carried out using two different pressure curves named according to their peak values as “172 bar” and “155 bar”, at operating point 1600 rpm and full load, where 1600 Nm brake torque is observed. The two pressure curves are given in **Figure 6.1**.

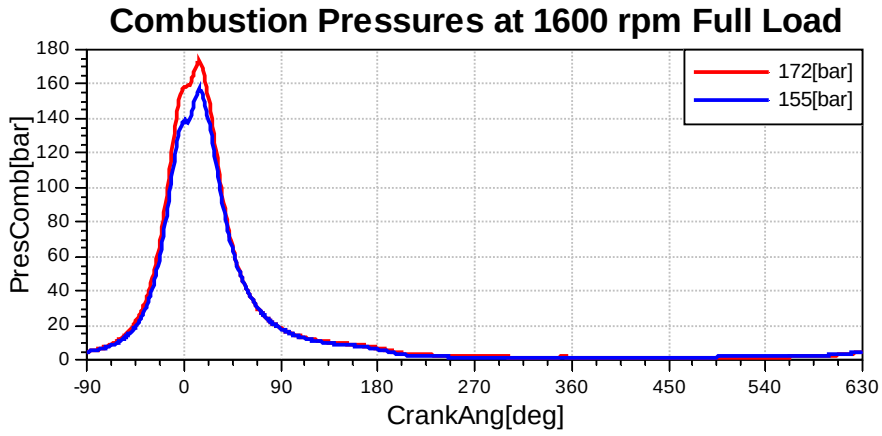

Figure 6.1: Combustion Pressure Excitation Curves with 172 bar and 155 bar Peak Firing Pressures

The predicted oil consumption values are depicted in **Figure 6.2**, **Figure 6.3, Figure 6.4 and Figure 6.5** as a summary according to different oil consumption sources.

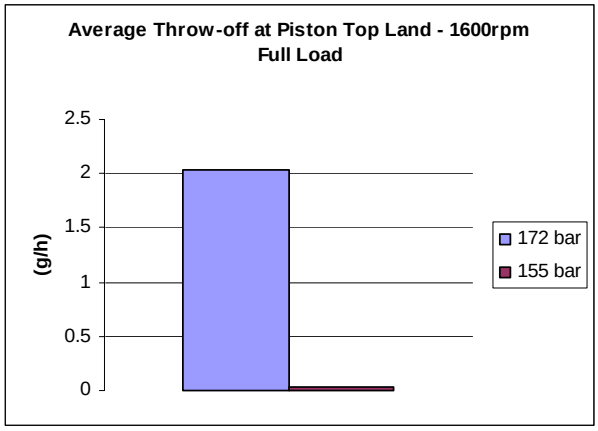

Figure 6.2: Average Throw-off at Piston Top Land

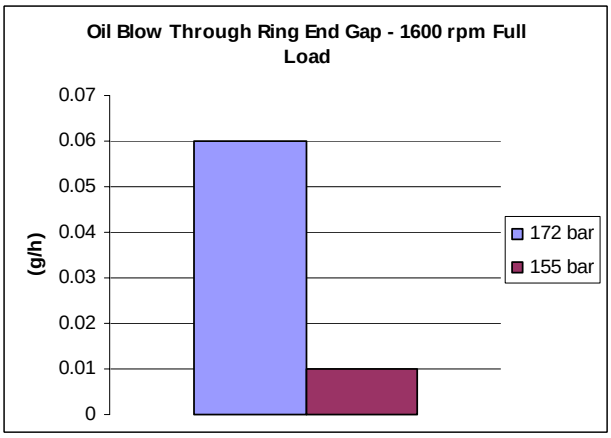

Figure 6.3: Oil Blow through Ring End Gap

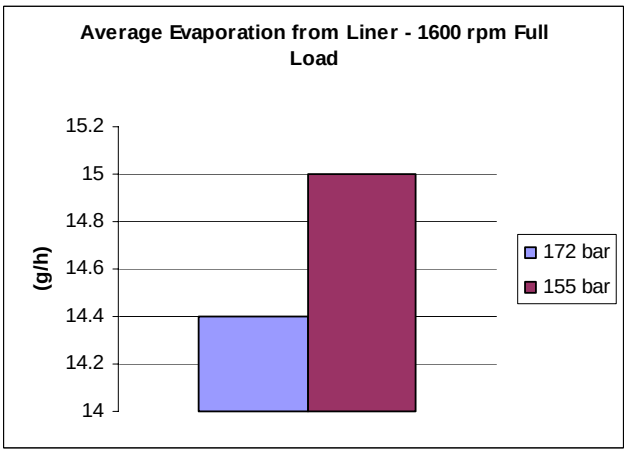

Figure 6.4: Average Evaporation from Liner

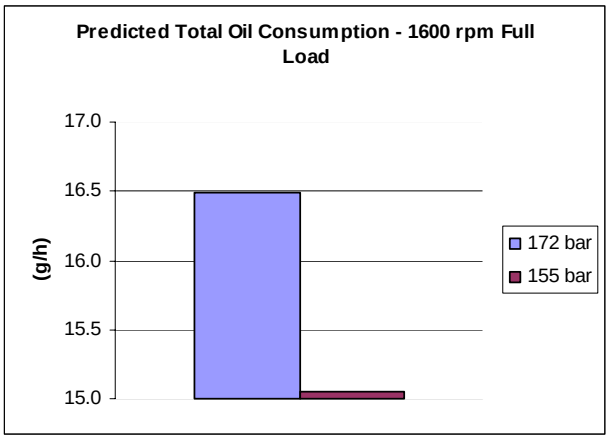

Figure 6.5: Total Oil Consumption

At 1600 rpm full load operating point, a decrease in total oil consumption is observed although significant difference is observed in individual oil consumption due to different sources. Generally oil consumption is predicted to increase by 5%, corresponding to a decrease in peak firing pressure by 10%, with oil consumption due to throw-off and evaporation are counteracting their trends. For a detailed analysis, piston dynamics, ring dynamics and distribution of oil consumption within engine cycles are analyzed in following sections.

6.1.1.1. Analysis of piston dynamics

While evaluating the results of piston dynamics calculations, it should be kept in mind that the crankshaft acceleration is assumed to be zero throughout the calculations. Therefore, any effect coming from the other five cylinders as speed fluctuation is ignored which is expected to introduce some additional difference in piston motion for different combustion pressures. This is due to the fact that speed fluctuation will be increased with increased peak firing pressure. The results of piston dynamics calculation is given in **Figures 6.6 and 6.7.**

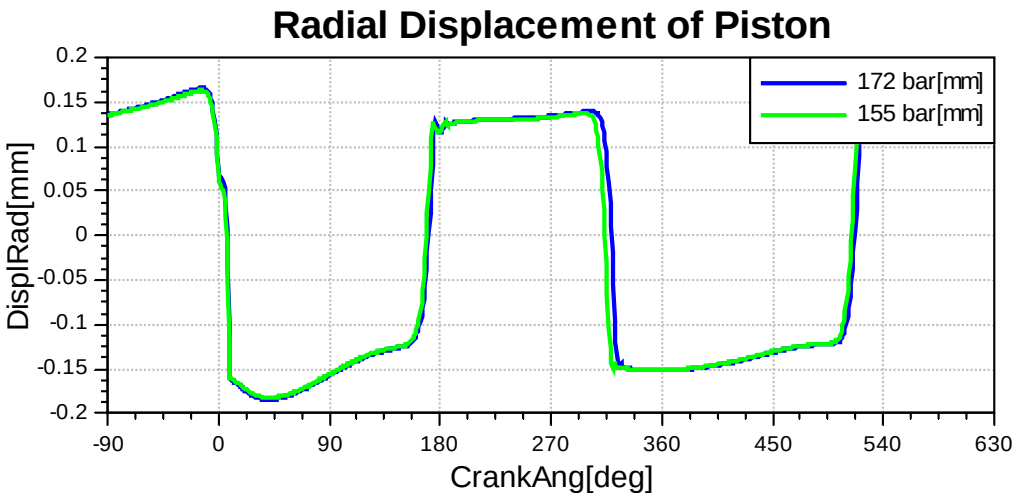

Figure 6.6: Radial Displacement of Piston Pin

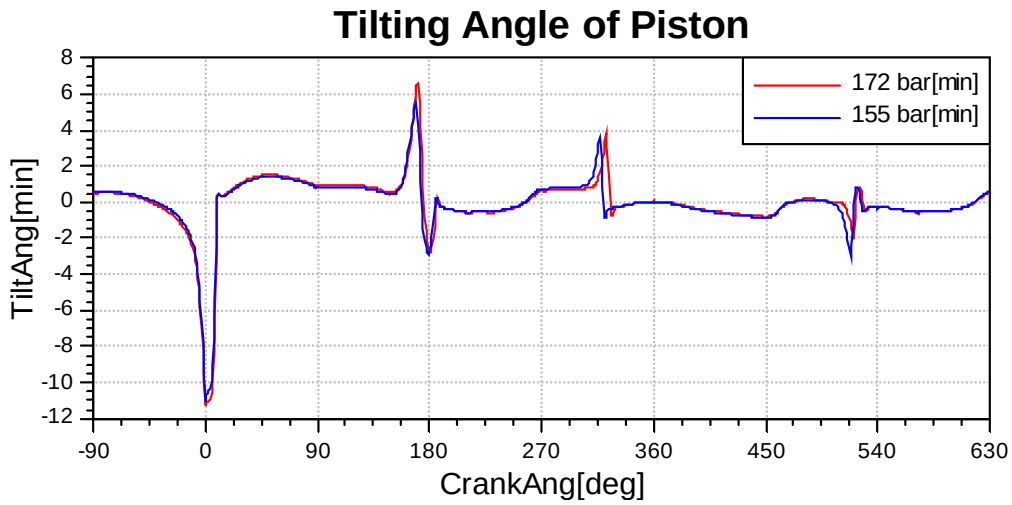

Figure 6.7: Tilting Angle of Piston

The results show that there is not a significant difference in piston radial displacement and very small difference in tilting angle of piston, where the difference arises due to response of relatively elastic piston skirt to decreasing excitation loads. Some difference may occur in piston slap forces, occurring due to contact of relatively stiff sections of the piston (piston crown) with liner, however, this is out of scope of this study. Therefore, the result from the piston dynamics simulation is that, since there is small difference in piston secondary motion, the influence of piston dynamics to ring dynamics will be the same in both cases. Hence any variation in ring dynamics between the thrust and anti-thrust sides should be more or less the same in two cases.

6.1.1.2. Analysis of ring dynamics and oil consumption

Pressures occurring in ring lands and axial motion of the rings are the most important output of the ring dynamics calculation, indicating the stability and characteristics of ring motion. It is generally possible to explain most of the oil consumption and blow-by trends just by analyzing these data. The pressure values occurring in the ring lands are given in **Figures 6.8 and 6.9** for 172 bar and 155 bar cases respectively. The results of ring motion calculations for 1600 rpm full load are given in **Figures 6.10, 6.11 and 6.12** comparatively for both cylinder pressure cases.

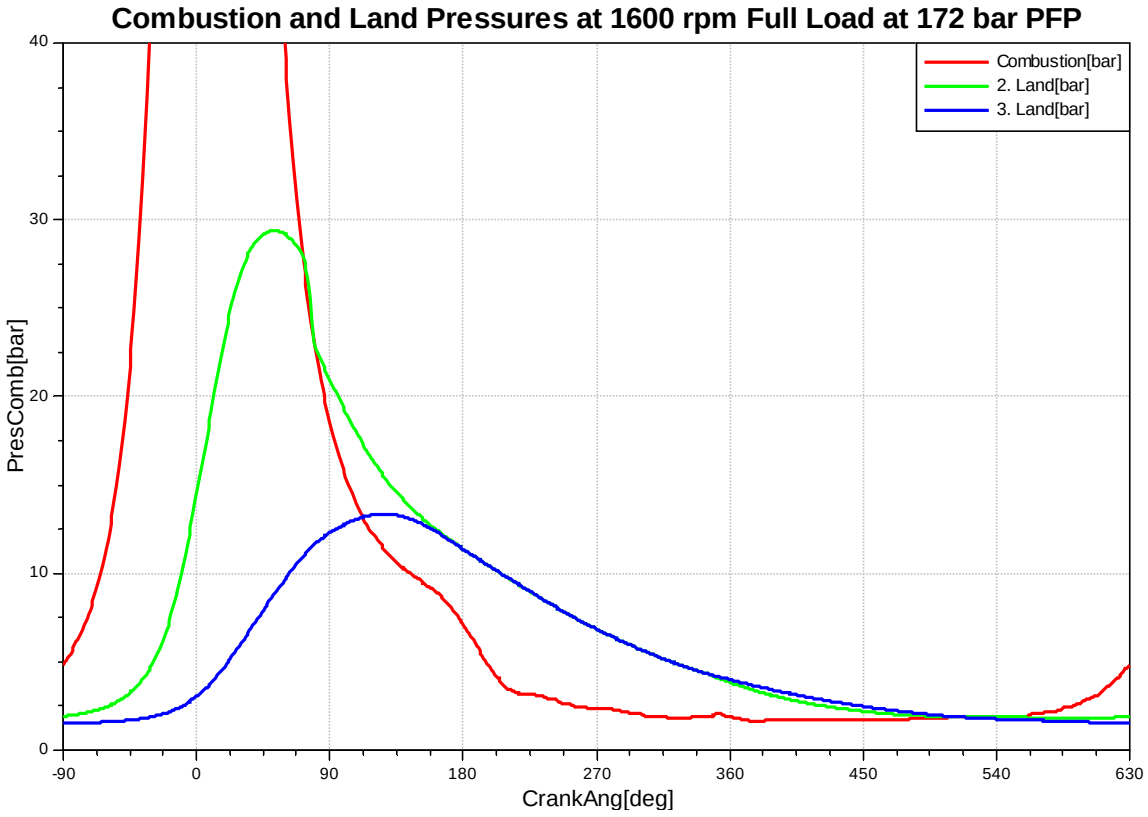

Figure 6.8: Combustion and Ring Land Pressures at 1600 rpm Full Load for 172 bar PFP

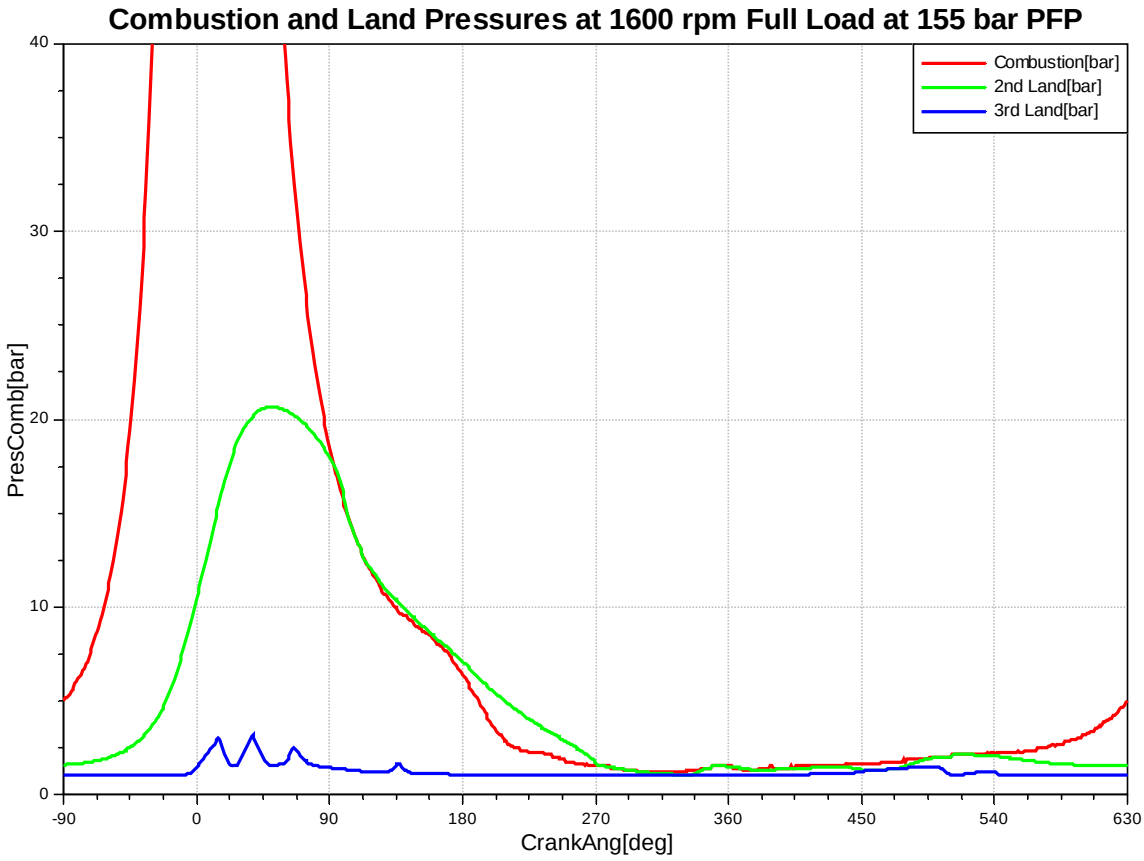

Figure 6.9: Combustion and Ring Land Pressures at 1600 rpm Full Load for 155 bar PFP

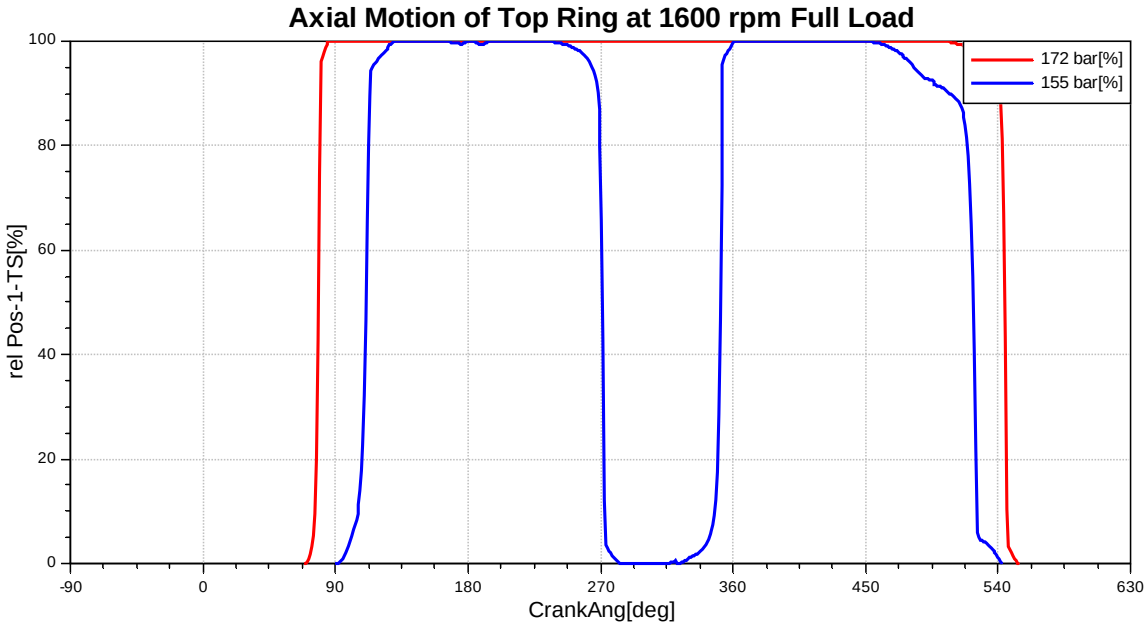

Figure 6.10: Relative Axial Position of Top Ring at 1600 rpm Full Load for 172 bar PFP

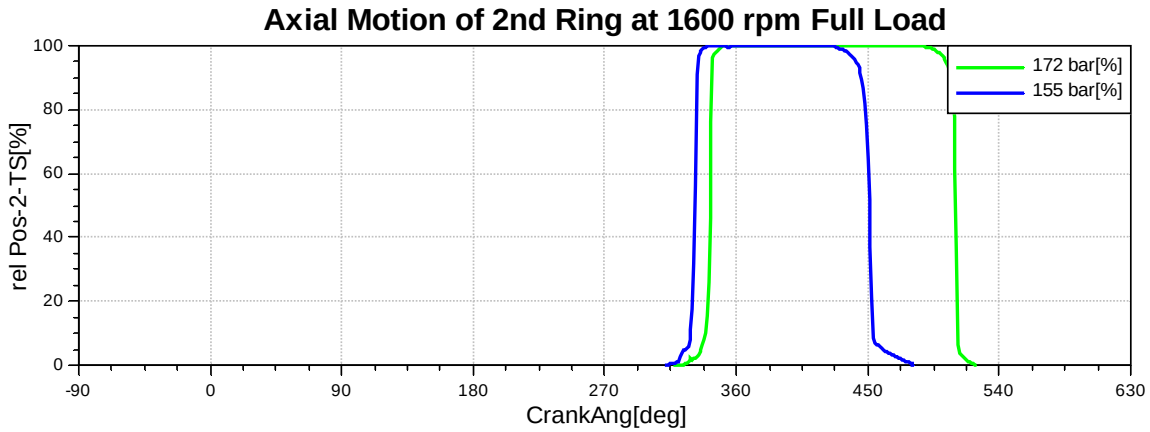

Figure 6.11: Relative Axial Position of 2nd Ring at 1600 rpm Full Load for 172 bar PFP

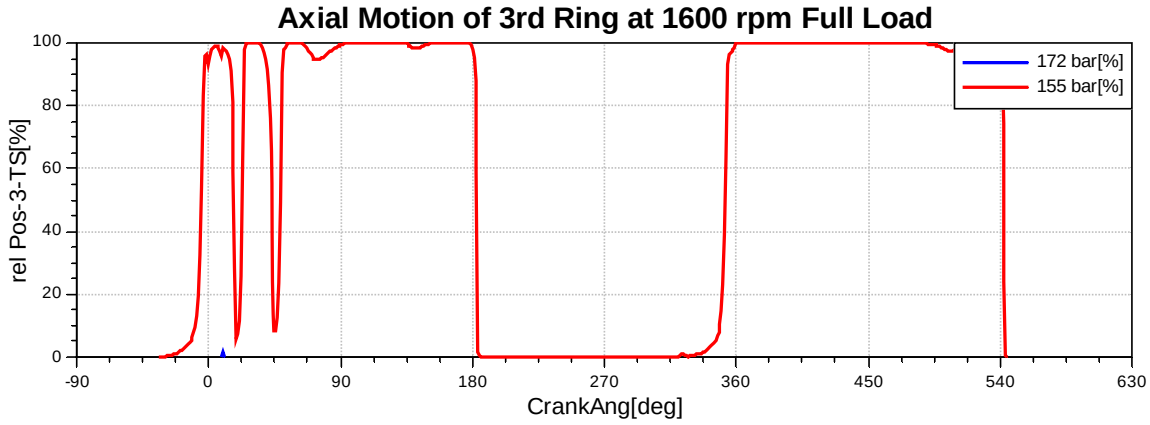

Figure 6.12: Relative Axial Position of Oil Ring at 1600 rpm Full Load for 172 bar PFP

It can be observed in **Figure 6.8** that second land pressure reaches a higher value than combustion pressure at about 60° after TDC, nearly till the end of intake stroke, for 172 bar PFP. Reverse gas flow occurs throughout this portion of the cycle. This is not a desired situation since the gas flowing from second land to combustion chamber can drag oil stream and cause oil consumption. In this case amount of oil in the second land is important and will be investigated later. The most important point to note is the very low activity of the oil ring. A tiny ring lift is observed at oil ring which is negligible, but gives a clue that the ring is in the onset of its lift with decreasing 3rd land pressure. This will be observed at 155 peak firing pressure. In 172 bar case, however, the 3rd land pressure is always enough to overcome inertial forces and ring sits at bottom groove flank. This stagnant state of the oil ring is very desirable from oil consumption point of view because there is always splashed oil below the oil ring and any motion of the oil

ring transports this oil by squeezing in the flanks to the upper regions of the piston and increases the tendency of oil to reach combustion chamber and compression rings.

At 172 bar peak firing pressure, top ring lifts only once at nearly 70° after TDC and resides at the upper groove until the end of intake stroke. Because of this motion 2nd land pressure follows combustion pressure closely until top ring lift and takes higher values as more gas flows into 2nd land through top ring groove when top ring occurs.

Since high pressure build-up occurs at 2nd land, second ring motion is also stable with only a single lift. Therefore, the ring seal well and allows the 2nd land pressure to rise higher than combustion pressure leading to reverse gas flow. This is the main reason of difference in thrown-off oil quantity between the two cases.

In **Figure 6.9**, it is shown that, when peak combustion pressure is lowered to 155 bar, 2nd land pressure is higher than combustion pressure for a lower period of the cycle (about 90° crank angle). In general, 2nd land pressure in 172 bar case is higher than 155 bar case as expected, which leads to higher 3rd land pressure

The outstanding consequence of higher 2nd land pressure is reflected to oil consumption due to throw-off above top ring. Oil throw-off is determined merely by the accumulated oil above top ring and the acceleration of the ring. **Figure 6.13** reveals that more oil is accumulated on the top ring for 172 bar case, due to higher second land pressure, than 155 bar. Two-piece shape of the oil accumulation curve for 155 bar PFP shows that the main transport mechanism is the pumping action of top ring during ring lift, whereas in high firing pressure the major source is the reverse gas flow from end gap. As a result of higher amount of oil above top ring, oil consumption due to oil throw-off is significantly higher with 172 bar peak firing pressure. This is demonstrated in **Figure 6.14** below.

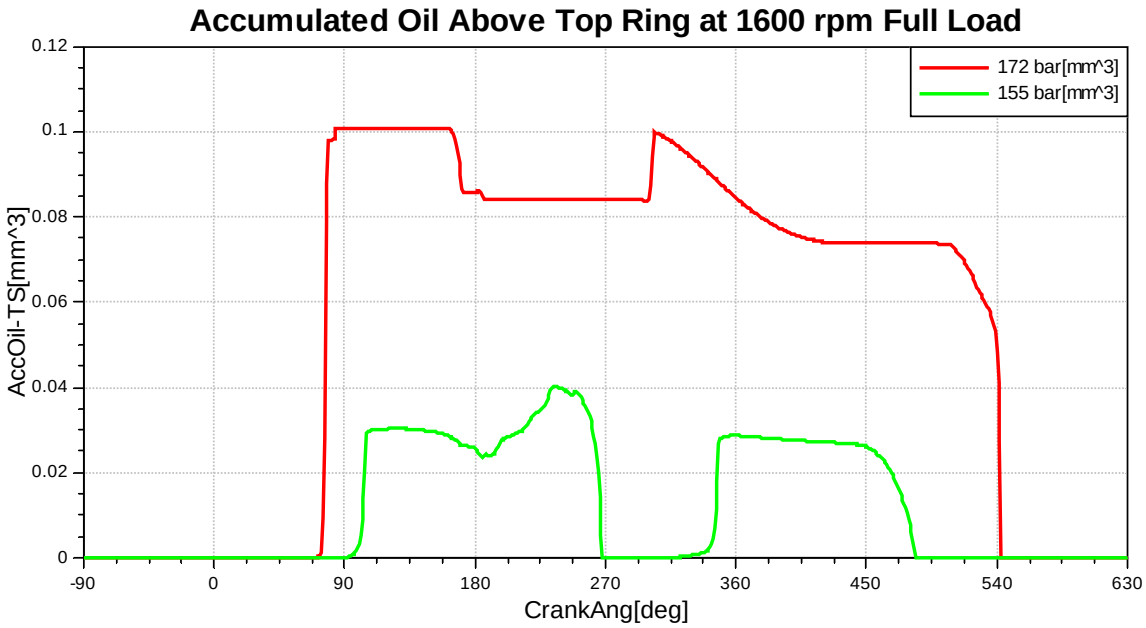

Figure 6.13: Accumulated Oil above Top Ring at 1600 rpm Full Load

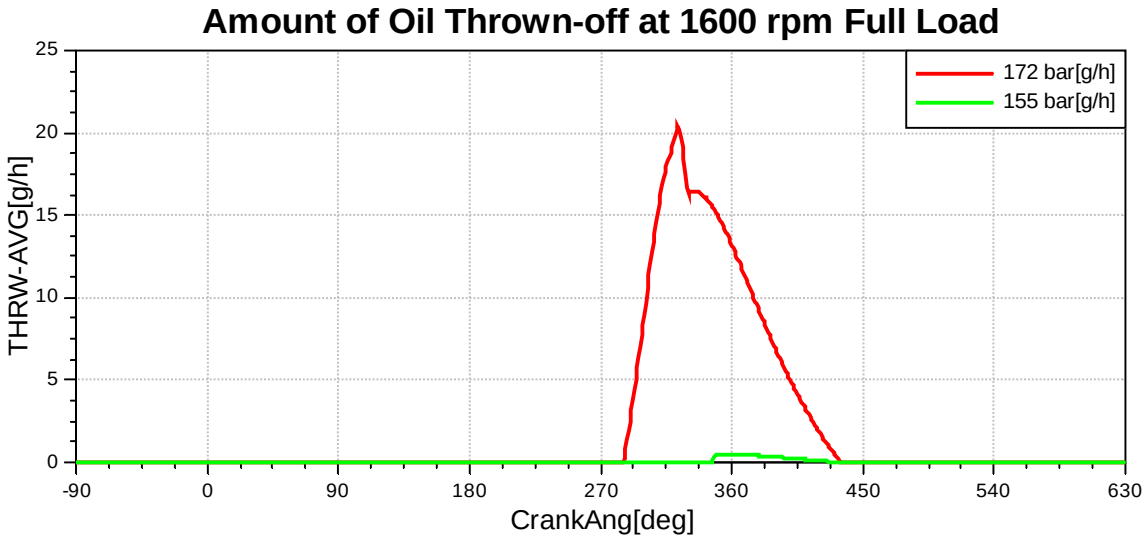

Figure 6.14: Amount of Oil Thrown-off at 1600 rpm Full Load

It should be noted that the top ring is only able to throw oil into the combustion chamber at the end of exhaust stroke, even though inertial forces and sufficient oil is present at the beginning of expansion stroke, since high combustion pressure counteracts and prevents inertial forces to shear oil from the surface into hot gas stream.

The variation in consumed oil amount due to evaporation is best explained by a comparison of oil film thickness on the liner since the liner temperature and combustion

gas temperature is kept constant. **Figure 6.15** provides a comparison oil film thickness left behind the top ring, which is calculated by simultaneous solution of average Reynolds's equation and equation of motion for piston ring.

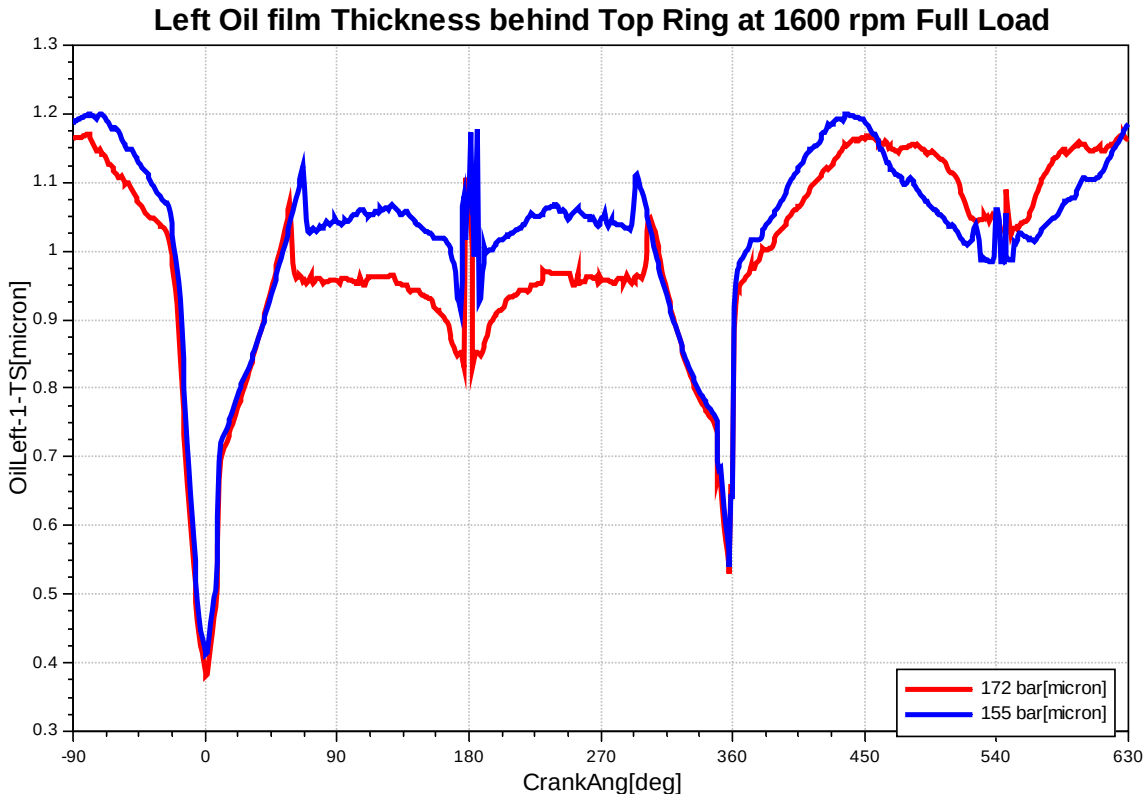

Figure 6.15: Left Oil Film Thickness behind Top Ring for 1600 rpm Full Load

The oil film layer, which is exposed to combustion and intake air, is thicker in a wide range of the engine cycle, which is the main reason for expected higher evaporation from liner. However, this effect is mostly diminished since the film thickness is almost the same when in-cylinder gas temperature is highest near TDC.

Finally, it is worth to analyze oil ring motion, as there is a huge difference between the two cases. While a weak flutter is observed in 155 bar case, the oil ring almost does not move from the lower flank in 172 bar case. The most striking effect of this motion is observed in flow of combustion gas into crankcase, i.e. blow-by, shown in **Figure 6.16** below.

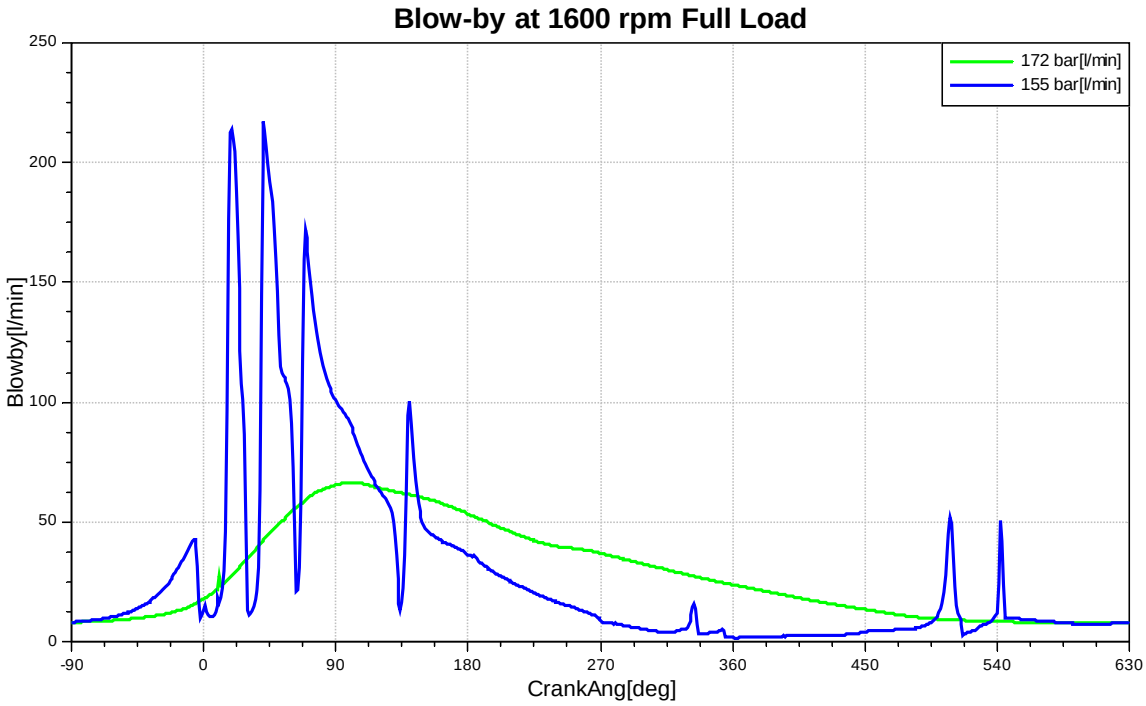

Figure 6.16: Blow-by at 1600 rpm Full Load

The unstable motion of the oil ring at 155 bar case is easily recognized from flow spikes in blow-by curve. The cumulative amount of blow-by is 169.2 l/min and 150.6 l/min for 172 bar and 155 bar respectively. Although it is possible to measure gas flow into crankcase by a simple gas flow meter, it is not possible to measure neither this flow nor crankcase pressure instantaneously, since high capacity of crankcase and local effects make this measurement extremely hard.

It should also be noted that, despite the fact that cumulative blow-by rates are not very far, the quality of blow-by gas is quite different. Firstly, in 155 bar case blow-by occurs as high spikes, which means very high fluid velocity. This may cause pulverization of oil into the crankcase like a spray and leads to increased amount of small oil droplets in the crankcase gas, which is undesirable from crankcase ventilation point of view, because considering current crankcase ventilation technologies, no matter whether it is cyclone type or media type, the finer the droplet size is, the lower the efficiency.

To conclude, the characteristics of ring motion and land pressure differ dramatically with a variation in peak combustion pressure at 1600 rpm full load operating point.

Unstable oil ring behavior is observed with a scattered blow-by behavior as a consequence.

Predicted total oil consumption is not altered significantly, although oil transport and oil consumption due to oil throw-off is triggered with a reduced peak firing pressure of 155 bar.

The main reason for different land pressure and oil consumption due to throw-off is mainly the twice lifting of top ring in 155 bar case, as opposed to the single lift in 172 bar case.

6.1.2. 2200 rpm full load operating point

Two simulations have been carried out using two different pressure curves named according to their peak values as “172 bar” and “155 bar”, at operating point 2200 rpm and full load, where 1270 Nm brake torque is observed. The two pressure curves are given in **Figure 6.17.**

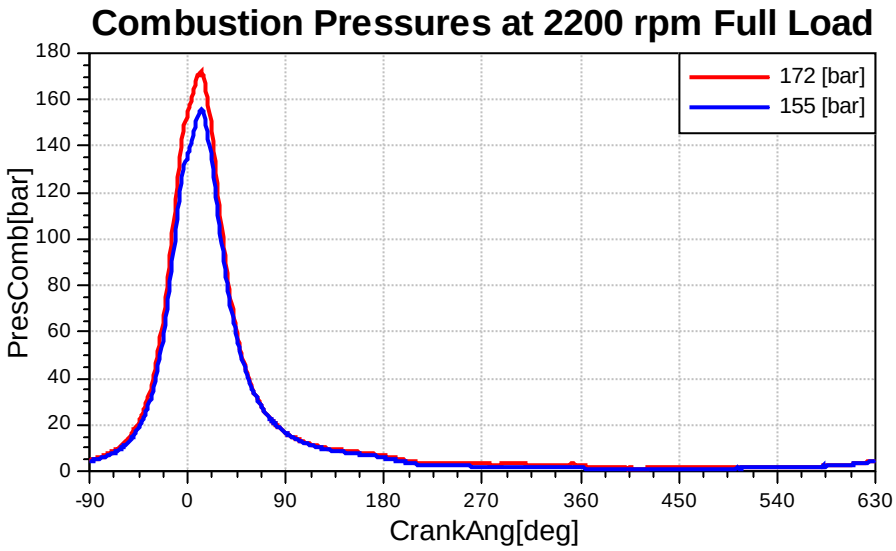

Figure 6.17: Combustion Pressure Variants at 2200 rpm Full Load

The predicted oil consumption values are depicted in **Figures 6.18, 6.19, 6.20 and 6.21** as a summary according to different oil consumption sources.

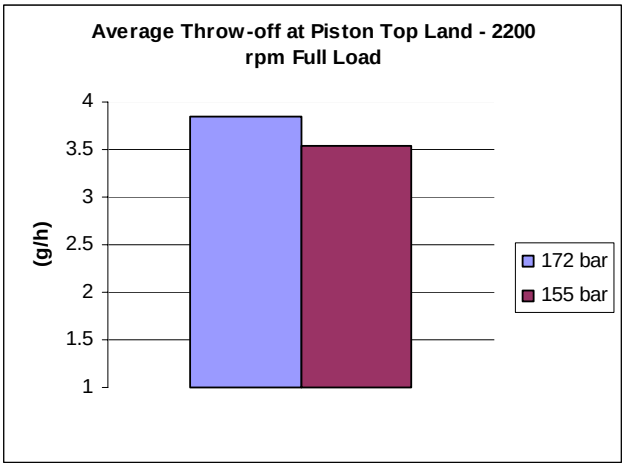

Figure 6.18: Average Throw-off at Piston Top Land

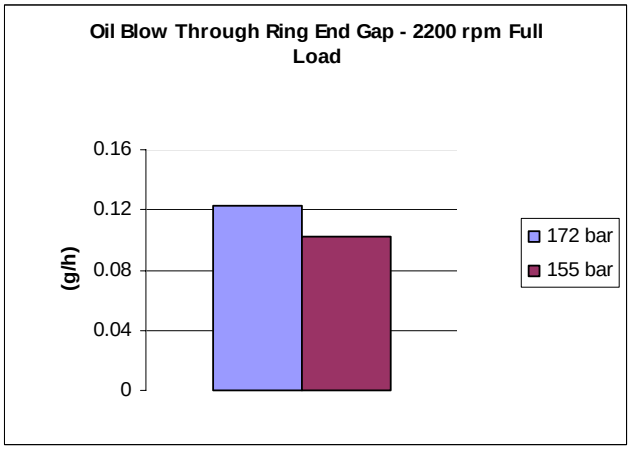

Figure 6.19: Oil Blow through Ring End Gap

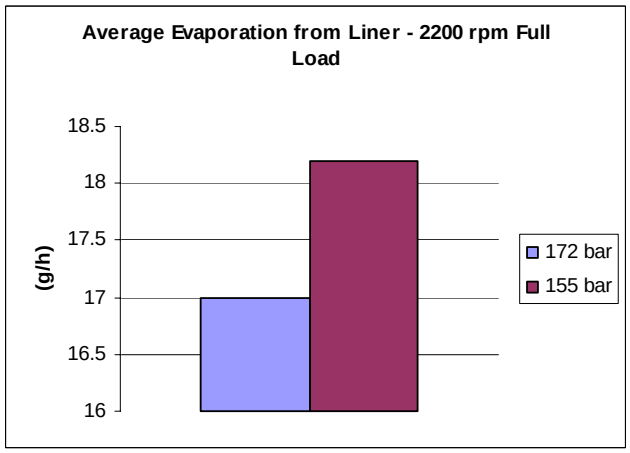

Figure 6.20: Average Evaporation from Liner

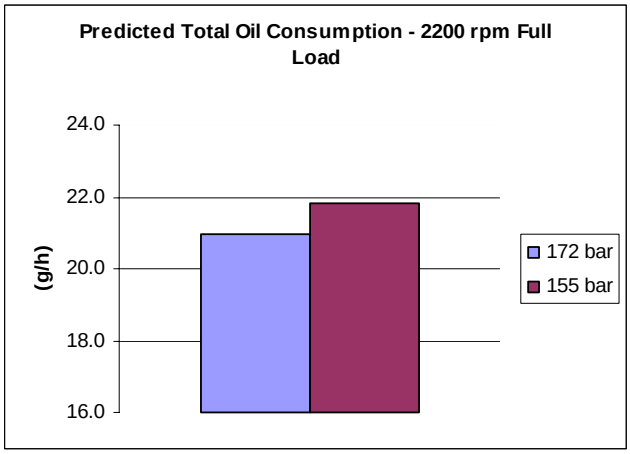

Figure 6.21: Total Oil Consumption

At 2200 rpm full load operating point, calculation results do not show a significant difference in oil consumption in total and in individual oil consumption sources. However, interestingly different characteristics are observed in ring dynamics which are analyzed in detail.

6.1.2.1. Analysis of piston dynamics

The radial displacement and piston tilting results of piston dynamics calculation is shown in **Figures 6.22and 6.23** with comparison of 172 bar peak firing pressure and 155 bar peak firing pressure variants.

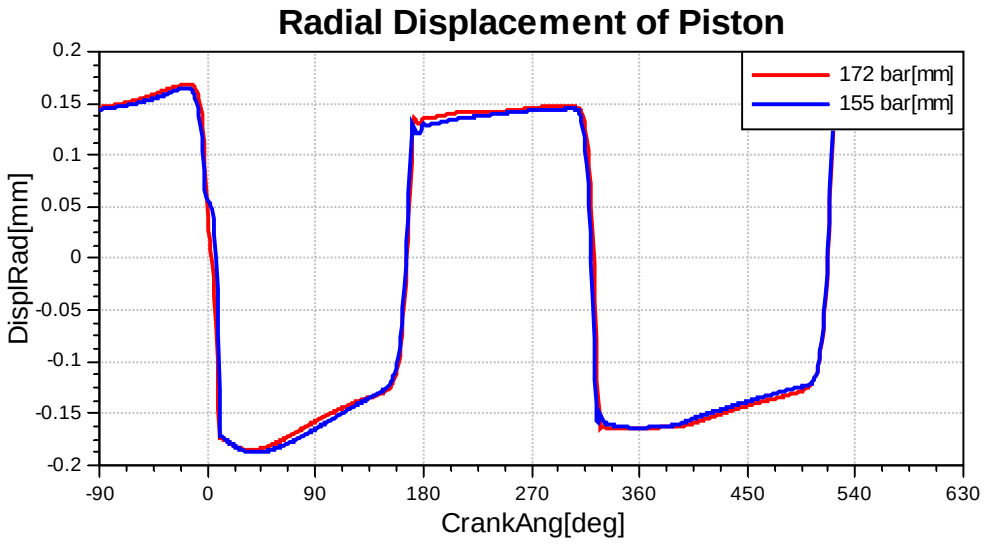

Figure 6.22 Radial Displacement of Piston

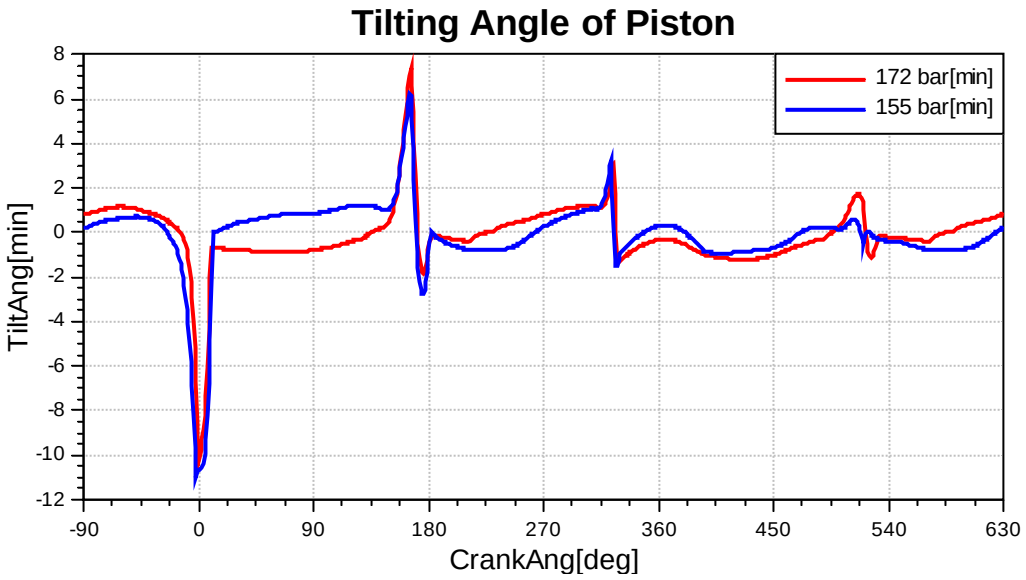

Figure 6.23 Tilting Angle of Piston

As opposed to the case in 1600 rpm, piston motion differs significantly, especially in expansion stroke. The motion may be considered to be altered in minor extend from piston slap point of view, however, the variation is of interest from ring dynamics and gas flow point of view, the reason is being the change in the sense of piston tilting just after firing in expansion stroke. Thus, the piston to liner clearances, ring twist and gas flow area at groove flanks are expected to be significantly different between the two cases. Therefore, while the effect of PFP is investigated, piston ring dynamics analysis has to be made both in thrust and anti-thrust sides at 2200 rpm full load operating point.

6.1.2.2. Analysis of ring dynamics and oil consumption

The calculated inter-ring pressures and ring motions for 2200 rpm full load operating point are shown in **Figures 6.24, 6.25**, and ring motions are given in Figures **6.26, 6.27, 6.28**. Since significant variation in piston secondary motion is observed between two different pressure cases, ring motions are analyzed both in thrust and anti-thrust sides. This was not seen to be necessary in 1600 rpm operating point since almost no difference was observed in piston movement.

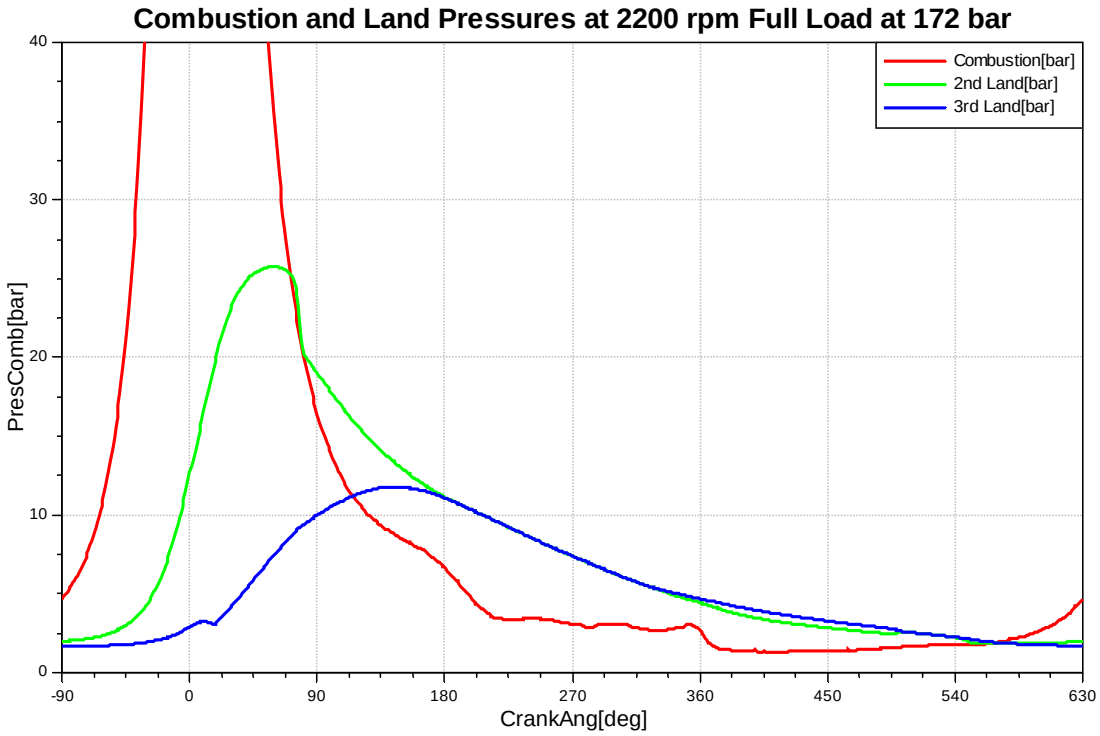

Figure 6.24 Combustion and Inter-ring Pressures at 2200 rpm Full Load for 172 bar PFP

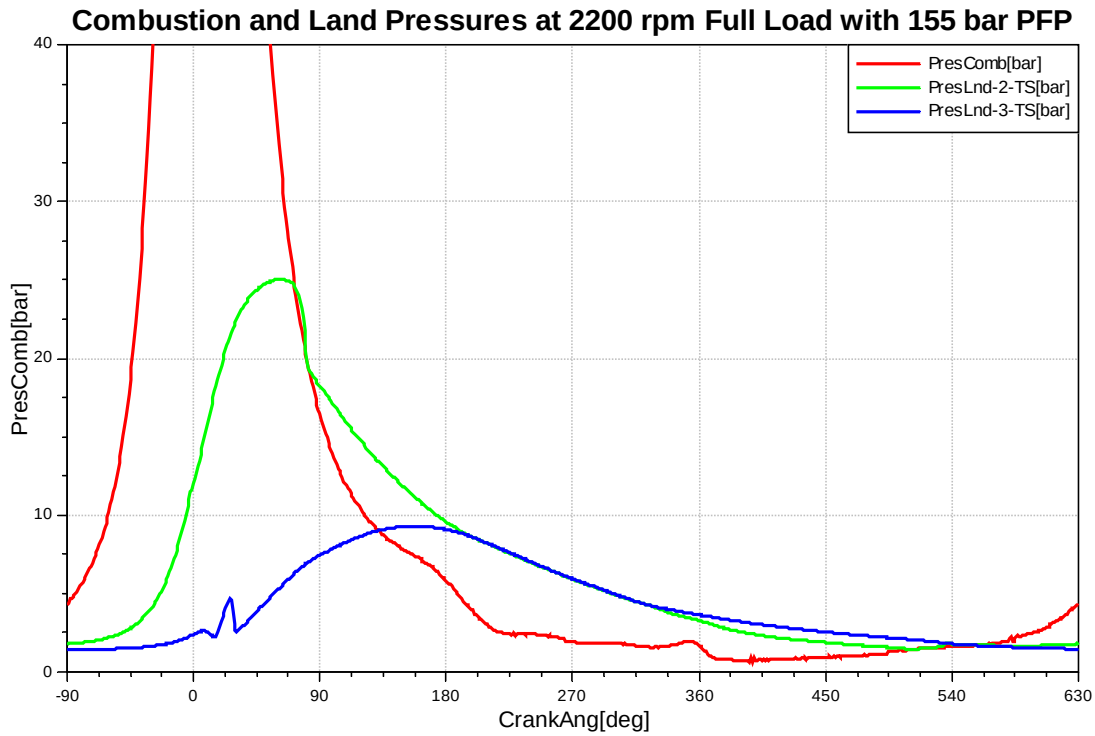

Figure 6.25: Combustion and Inter-ring Pressures at 2200 rpm Full Load for 155 bar PFP

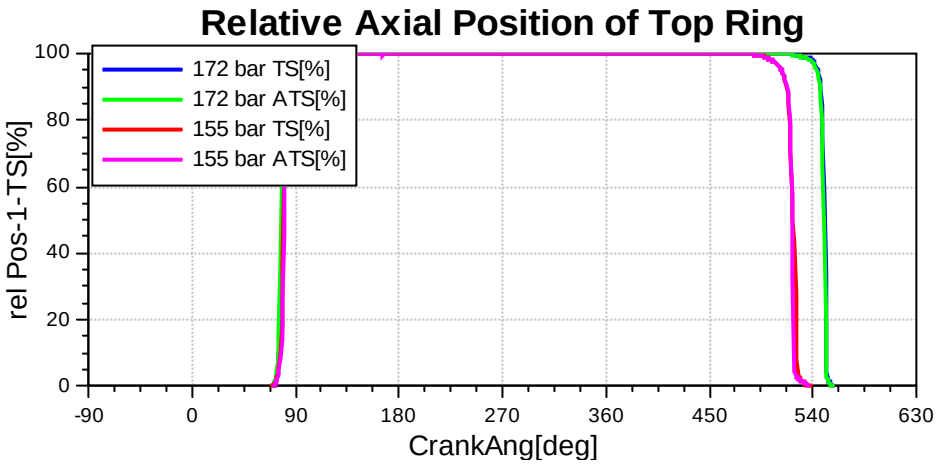

Figure 6.26: Relative Axial Position of Top Ring at 2200 rpm Full Load

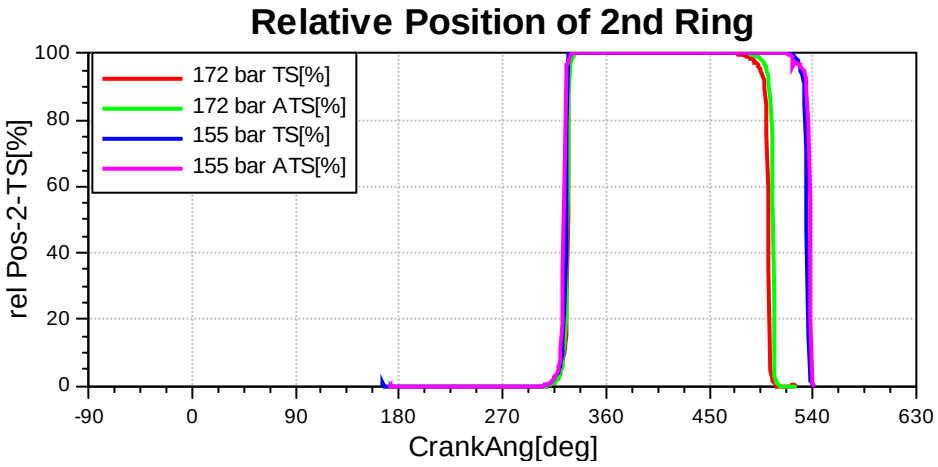

Figure 6.27: Relative Axial Position of 2nd Ring at 2200 rpm Full Load

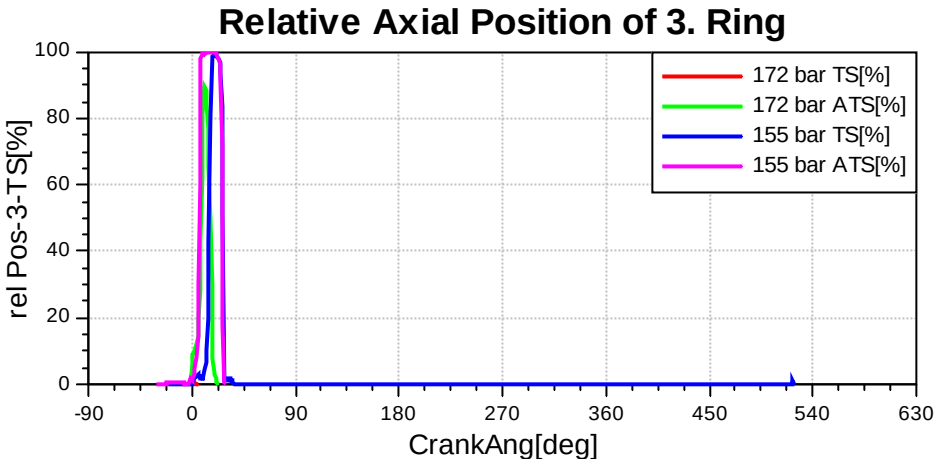

Figure 6.28: Relative Axial Position of 3rd Ring at 2200 rpm Full Load

The most dramatic effect in ring dynamics, due to combustion pressure alteration is observed at the oil ring axial motion. Oil ring exhibits a single lift only in the anti-thrust side in 172 bar case while preserving its position at the bottom groove flank at thrust side. However, in 155 bar case the two sides move together and ring lift occurs at both sides of the piston, allowing more gas flow area. This also leads to smaller ring twist of oil ring because the greater the deviation of axial motion from one side of the ring to the other, the greater the ring twist angle, although ring twist is also influenced by friction and damping forces. A comparison of ring twist angles of oil rings for the two cases are shown in **Figures 6.29 and 6.30.**

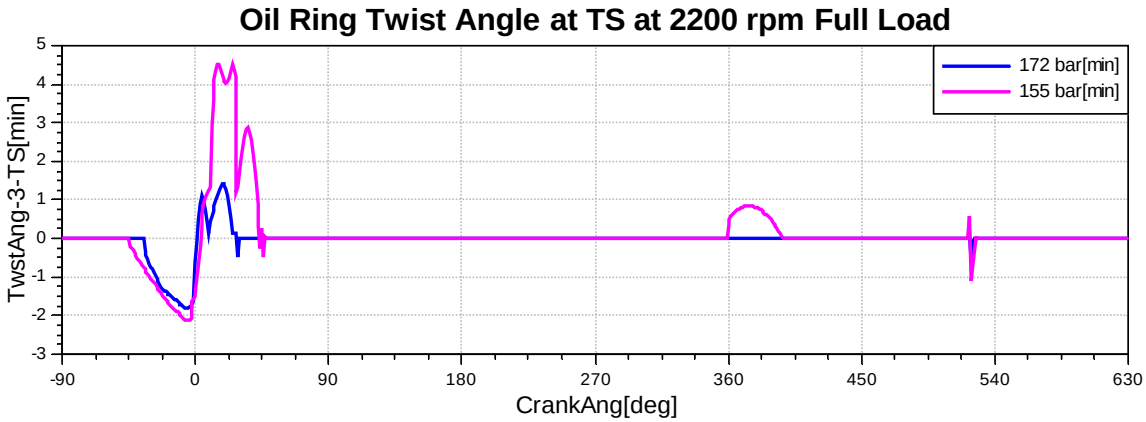

Figure 6.29: Comparison of Oil Ring Twist Angle as TS at 2200 rpm Full Load

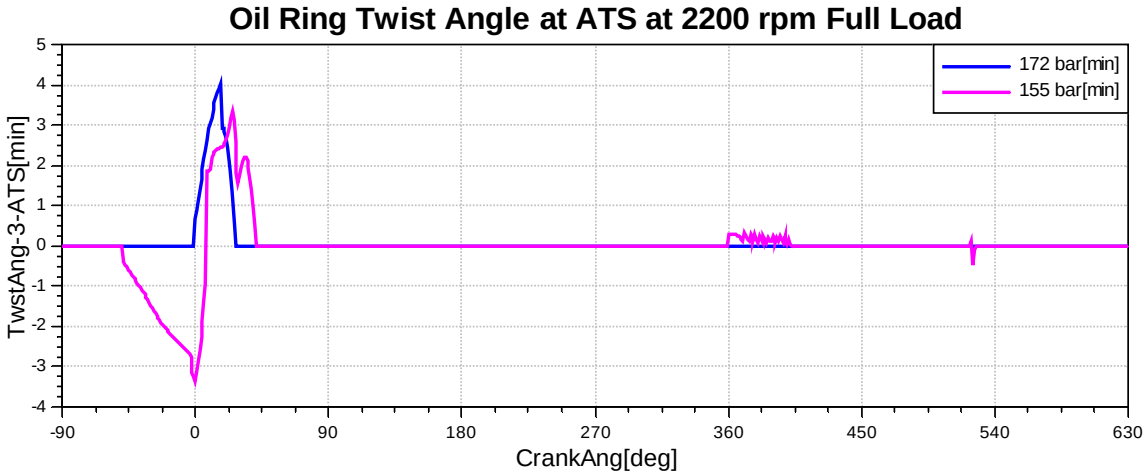

Figure 6.30: Comparison of Oil Ring Twist Angle as TS at 2200 rpm Full Load

The effect of oil ring motion is also apparent in blow-by behavior, which is shown in **Figure 6.31**. Gas flow into crankcase makes a higher jump at TDC for 155 bar as a

result of ring lift in both sides and relieves the pressure in 3rd land. Because of less pressure build up at 3rd land in 172 bar case, gas flow through ring end gap is less. See references for more information about ring twist effects on oil ring function **(Tian and Wong, 2000)**

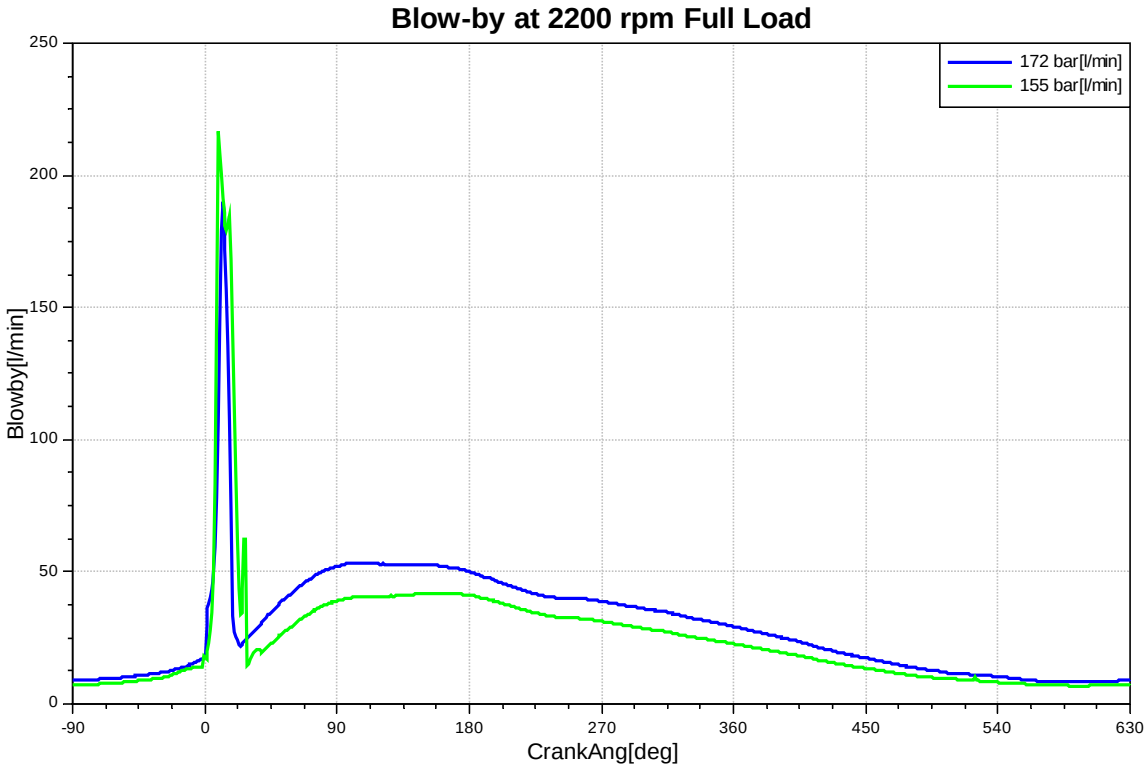

Figure 6.31: Blow-by at 2200 rpm Full Load

Top ring motion differs only by an advance of 40-45° of settling to bottom groove, with increasing peak firing pressure. This causes a small increase in second land pressure together with retardation in second ring settling. The double lifting of the top ring is not observed in 2200 rpm case, as it was in 1600 rpm case, because the higher inertial forces assist 2nd land pressure to hold top ring at upper groove throughout the expansion and intake strokes.

Finally, it is worth to add a few words about oil consumption to top land scraping oil consumption mechanism. Since the deposit thickness at top land of the engine, on which the experimental work has been carried out, was not known, oil consumption due to top land scraping has not been included in the calculation model. Because once the deposits reach a level to contact the oil film on the liner, top land scraping oil consumption

mechanism is active and it is too sensitive to deposit thickness to model efficiently with considerable error. However, since the piston motion is altered, it can be concluded that for a given deposit height, that is high enough to trigger top land scraping (about 0.9 mm), high difference in oil consumption may be observed.

6.2. Experimental Investigation

6.2.1. Experimental method

The real-time oil consumption measuring system which uses SO_2 tracing technique has been used to detect the variation in lube oil consumption of Ecotorq 9.0 Liter heavy-duty diesel engine.

The experimental investigations have been established in two stages because of the reason that a cylinder pressure indicating system was not available in Automotive Technology Research and Development Center (OTAM) which is located in Istanbul Technical University Ayazağa Campus.

In the first stage, the cylinder pressure has been measured using AVL uncooled piezoelectric pressure sensor and AVL Indiset 620 as data acquisition, signal conditioning and amplifying system in Engine Laboratory of Product Development Test Center in Ford Otomotiv Sanayi A.Ş. Gölcük Plant. More information on cylinder pressure measurement has been given in **Section 5.2**. In this stage it is aimed to determine the calibration settings that will give the cylinder pressure curves with desired peak firing pressures and to record these cylinder pressure curves in order to use as excitation input for calculations presented above. This is accomplished by establishing a connection to Electronic Control Unit (ECU) of the engine, during engine operation on the AC dynamometer, to monitor and modify injection parameter settings while cylinder pressure is simultaneously measured.

The desired peak firing pressures can be obtained by varying three main injection parameters as injection timing, rail pressure and injected fuel quantity, with all engine hardware (especially turbo charger and inter-cooler which affect cylinder pressure) being the same. Among the three, the injected fuel quantity is the main factor that determines the operating point as it is the parameter that determines the torque output of

the engine. Therefore, it is kept constant unless a change in engine torque is observed when the other two parameters have been modified. In such a case torque can be corrected to its previous value by a small change in injected fuel quantity. This small change in injected fuel quantity does not affect cylinder pressure significantly, so iteration is not necessary. Furthermore, since engine-out emissions are not of interest during this study, it is sufficient to keep rail pressure at a certain value, and cylinder pressure can be changed by playing with injection advance.

As a result of the study at this stage, the following parameters have been found to yield the cylinder pressure curves with desired peak firing pressures and shown in **Table 6.1.**

Table 6.1: Calibration Settings for Desired Peak Firing Pressures

Operating Point	**Peak Firing Pressure (bar)**	**Injection Timing (DCA)**	**Rail Pressure (Mpa)**
1600 rpm 1570 Nm	172	-10	135
1600 rpm 1570 Nm	155	-5	135
2200 rpm 1240 Nm	172	-12	147
2200 rpm 1240 Nm	155	-7.4	147

In the second stage in OTAM engine laboratory, connection to the ECU is established to vary calibration parameters during engine operation and oil consumption is measured simultaneously. In this manner, it is possible to implement any change in engine management parameters online during engine operation and detect the changes in monitored oil consumption in real-time.

6.2.2. Experimental results

Oil consumption measurements have been performed with two peak firing pressures in two operating points as 2200 rpm and 1600 rpm at full load.

6.2.2.1. 1600 rpm full load operating point

Oil consumption measurements have been taken for 60 seconds for each peak firing pressure. The measured oil consumption results are comparatively shown in **Figure 6.32** below.

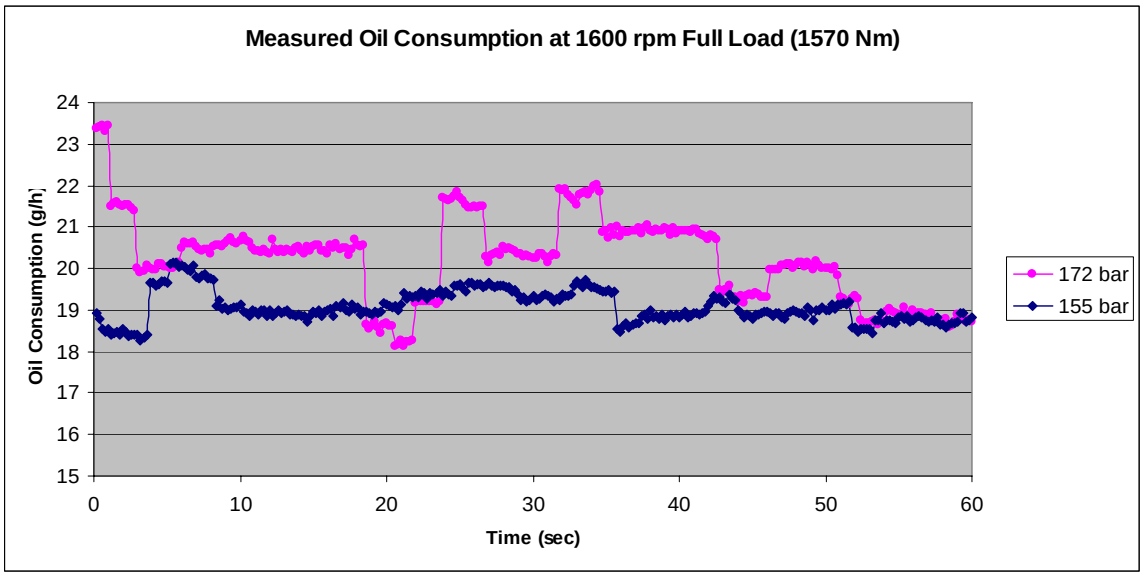

Figure 6.32: Oil Consumption Behavior at 1600 rpm Full Load with Two Different Peak Firing Pressures

As can be seen in Figure 37, the measurements show that, the difference between the oil consumption characteristics with 172 bar PFP and 155 bar PFP is not large enough compared to the inherent variation in the measurement. Therefore, significant difference in oil consumption is not observed between the PFP's of 172 bar and 155 bar, at 1600 rpm full load operation.

A comparison of oil calculated and measured oil consumption trends based on PFP is given in **Figure 6.33.**

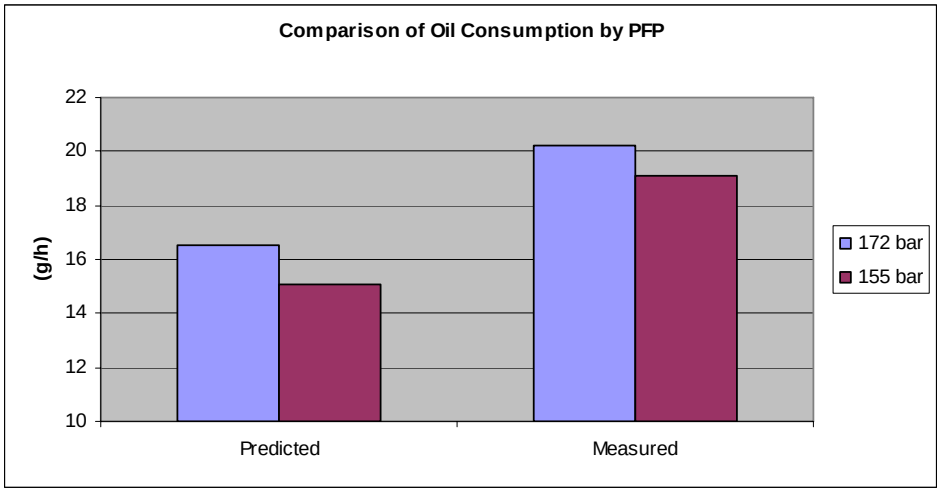

Figure 6.33: Comparison of Calculated and Measured Oil Consumption at 1600 rpm Full Load

It can be concluded at first look that both calculated and measured values show a decreasing trend with decreasing PFP. However, it should be noted that the differences in both cases are quite small to reach to a generalization. The trend in predicted values may be considered as significant, whereas the scatter and variation is higher in experimental conditions and contains lot of lurking variables such as cylinder roundness, T/C oil consumption and lost amount of burned oil through blow-by. Therefore, only a drastic change in measured oil consumption could be considered to reflect a difference between the two cases.

The absolute values of predicted and measured quantities also differ and it should be noted that measured values are always higher as expected since calculation consider a lot of idealizations and assumptions (round liner, and normal liner surface roughness) which leads to lower than actual predicted values.

6.2.2.2. 2200 rpm full load operating point

Oil consumption measurements have been taken for 60 seconds for each peak firing pressure. The measured oil consumption results are comparatively shown in **Figure 6.34** below.

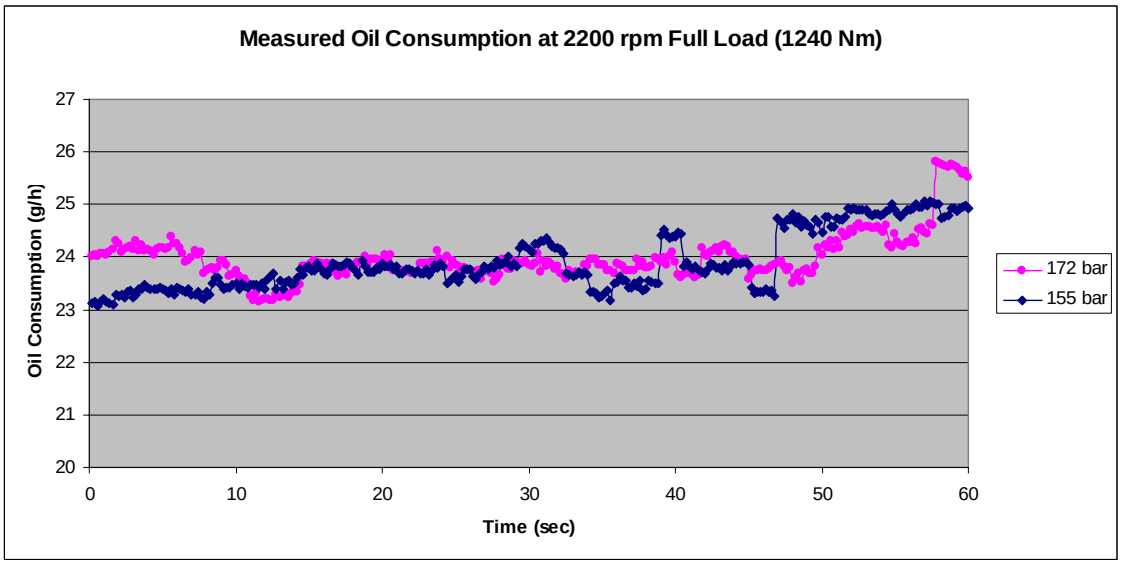

Figure 6.34: Oil Consumption Behavior at 2200 rpm Full Load with Two Different Peak Firing Pressures

As can be seen in Figure 37, the measurements show that, the difference between the oil consumption characteristics with 172 bar PFP and 155 bar PFP is not large enough compared to the inherent variation in the measurement. Therefore, significant difference in oil consumption is not observed between the PFP's of 172 bar and 155 bar, at 1600 rpm full load operation.

A comparison of oil calculated and measured oil consumption trends based on PFP is given in **Figure 6.35**.

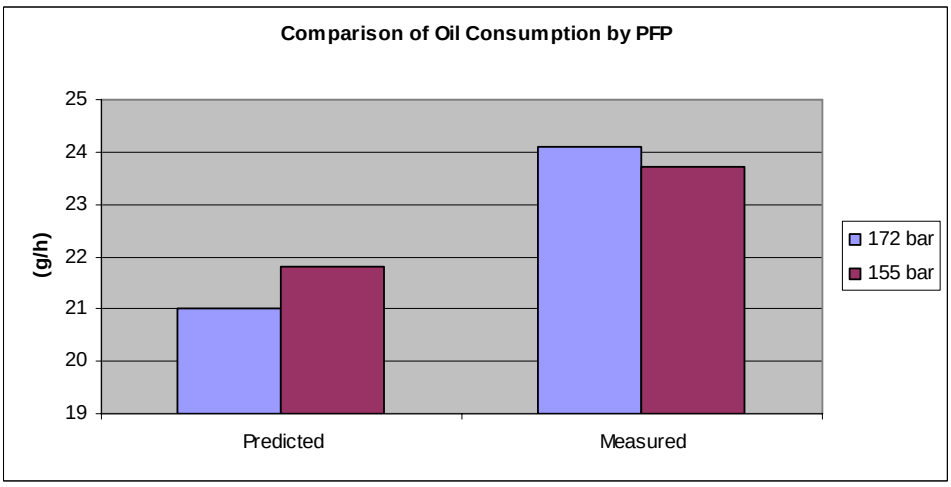

Figure 6.35: Comparison of Calculated and Measured Oil Consumption at 2200 rpm Full Load

In contrary to previous operating point, predicted and observed values show opposite trends. However, because of reasons mentioned above, the differences in measured quantities are not significant compared to the accuracy and precision of oil consumption measurement.

7. CONCLUSION AND DISCUSSIONS

In this thesis, the effect of peak cylinder pressure on engine oil consumption is assessed in two parts. Firstly, a theoretical model is constructed using AVL Glide in order to predict piston dynamics, ring dynamics and consequently lube oil consumption of Ecotorq 9.0 L heavy-duty diesel engine. Several simulations are performed in rated power (2200 rpm full load) and maximum torque operating conditions for two cylinder pressure cases, characterized according to their peak values as 172 bar and 155 bar. Then, an experiment is designed and performed to measure the effect of cylinder pressure on lube oil consumption. These cases are demonstrated in actual engine operation by on-line connection to engine ECU and changing injection advance. Real-time engine oil consumption is measured by using SO_2 tracing technique.

Analytical investigations have shown that gas flow through the rings, inter-ring pressures and ring motions are significantly affected by peak cylinder pressure both in quantitative and qualitative point of view. The effect is especially dominant at mid speed, i.e. 1600 rpm full load case, since the dynamics are more influenced by gas excitation rather than moderate speed. At this operating point, twice lifting of the top ring is seen to disappear with increasing PFP due to an increase in second land pressure. The flutter behavior of the oil ring also disappears with increasing cylinder pressure, since the increasing 3rd land pressure is sufficient to keep the ring in the lower flank of the ring groove. As a result of different oil ring motion the blow-by characteristics also change and blow-by flow becomes more uniform as ring flutter ceases. The oil consumption by oil-throw of from top ring becomes active with increased cylinder pressure as the early pressure build-up at 2nd land and steeper descending of combustion pressure results in reverse gas flow into combustion chamber. However, considering oil consumption figures, a significant change has not been observed. This very low sensitivity of oil consumption to ring dynamics is considered to be a weakness of the

model. On the other hand, the high difficulty in modeling such a very complex phenomenon like oil transport should be appreciated.

The influence of cylinder pressure on ring dynamics seems to diminish with increasing speed, which leads to the conclusion that there is a two-way interaction between PFP and engine speed when ring response is considered. However, the oil ring lifting characteristic is also altered as a result of increasing 3rd land pressure. At high engine speed, it is predicted that, unlike mid-speed condition, the piston motion also change considerably. This influences the interaction between the thrust and anti-thrust sides of the piston. It should also be considered that after long engine operation when the topland deposits came into the picture, the oil consumption characteristics nay differ considerably with changing piston secondary motion. This is due to the fact that topland scraping becomes the dominant oil consumption mechanism when it is active. Again, at this operating point a significant difference in oil consumption is not predicted for different peak firing pressures.

A significant influence on oil consumption is also not observed as a result of real-time oil consumption measurements, in both load cases.

To conclude, a theoretical oil consumption model and real-time oil consumption measurement are performed to asses the effects of PFP on engine lube oil consumption. Although theoretical study shows significant influence on ring dynamics, neither analytical investigation nor experimental data show a considerable effect on oil consumption.

REFERENCES

Ariga, S., 1996. Observation of Transient Oil Consumption with In-Cylinder Variables, *SAE Paper,* **961910.**

Ariga, S., Sui, P. C. and Shahed, S. M., 1992a. Instantaneous Unburned Oil Consumption Measurement in a Diesel Engine Using SO2-Tracer Technique, *SAE Paper* **922196.**

Ariga, S., Sui, P. C., Bailey, B., Kumakiri, T., Osumi, Y. and Sakamoto, A., 1992b. On-Line Oil Consumption Measurement and Characterization of an Automotive Gasoline Engine by SO2- Method, *SAE Paper* 920652

Audette, W.E. and Wong,V.W., 1999. A Model For Estimating Oil Vaporization From The Cylinder Liner As A Contributing Mechanism to Engine Oil Consumption**,** *SAE Paper,* **1999-01-1520**.

AVL Glide User's Manual, 2005. Piston Movement, AVL List GmbH.

AVL Glide User's Manual, 2005. Ring Dynamics and Lube Oil Consumption, AVL List GmbH.

Bailey, B. K. and Ariga, S., 1990. On-Line Diesel Engine Oil Consumption Measurement, *SAE Paper* **902113.**

Dursunkaya, Z. and Keribar, R., 1992. Simulation of Secondary Dynamics of Articulated and Conventional Piston Assemblies, *SAE Paper* **920484.**

Dursunkaya Z., Keribar, R., and Richardson, D. E., 1993. Experimental and Numerical Investigation of Interring Gas Pressures and Blow-by in a Diesel Engine, *SAE Paper,* **930792.**

Froelund, K., 1999. Real-Time Steady-State Oil Consumption Measurement on Commercial SI-Engine, *SAE Paper*, **1999-01-3461.**

Furuhama, S. and Hiruma, M., 1979. Piston Ring Motion and Its Influence on Engine Tribology, *SAE Paper* **790860.**

Greenwood, J. A., and Tripp, J. H., 1971, The Contact of Two Nominally Flat Surfaces, *Proc. Inst. Mech. Engrs*., Vol. **185**, p. 625.

Herbst , H. M., and Priebsch, H.H., 2000. Simulation of Piston Ring Dynamics and Their Effect on Oil Consumption, *SAE Paper,* **2000-01-0919.**

Inagaki, H., Saito, A., Murakami, M., and Konomi, T., 1995. Development of Two-Dimensional Oil Film Thickness Distribution Measuring System**,** *SAE Paper,* **952346.**

Keribar, R., Dursunkaya, Z., and Ganapathy V., 1993. An Integrated Design Analysis Methodology to Address Piston Tribological Issues**,** *SAE Paper,* **930793.**

Mihara, K., and Inoue, H., 1995. Effect of Piston Top Ring Design on Oil Consumption, *SAE Paper,* **950937.**

Nakashima, K., Ishihara, S., and Urano, K., 1989. Influence of Piston Ring Gaps on Lubricant Oil Flow into the Combustion Chamber, *SAE Paper,* **952546.**

Nakashima, K., and Ishihara, S., 1995. Influence of Piston Ring Gaps on Lubricating Oil Flow into the Combustion Chamber**,** *SAE Paper,* **952546.**

Patir, N., and Cheng, H. S., 1979, Application of Average Flow Model to Lubrication Between Rough Sliding Surfaces, *ASME Journal of Lubricaton Technology*, Vol. **101**, pp. 220-230.

Prata, A.T. and Fernandes, J. R.S., 2000. Dynamic Analysis of Piston Secondary Motion For Small Reciprocating Compressors**,** *ASME Journal of Tribology***,** Vol. **122,** pp. 752-760, 2000.

Rabuté, R. and Tian, T., 2001. Challenges Involved in Top Ring Designs for Modern SI Engines, *Journal of Engineering for Gas Turbines and Power*, Vol. **123,** pp. 448-459.

Rakopoulos, C.D., Hountalas D.T., Koutroubousis, A.P. and Zannis, T.C., 2001. Application and Evaluation of a Detailed Friction Model on a DI Diesel Engine with Extremely High Peak Combustion Pressures, *SAE Paper* **2002-01-0068.**

Thirouard, B., Tian, T., and Hart, D. P.,1998. Investigation of Oil Transport Mechanisms in the Piston Ring Pack of a Single Cylinder Diesel Engine, Using Two Dimensional Laser Induced Fluorescence, *SAE Paper,* **982658.**

Tian, T., Wong, V.W., Lang, H., and Ryan, J.P., 1994. A Numerical Model of Piston Secondary Motion and Piston Slap in Partially Flooded Elastohydrodynamic Skirt Lubrication , *SAE Paper,* **940696**.

Tian, T., Wong, V.W., 2000. Modeling the Lubrication, Dynamics, and Effects of Piston Dynamic Tilt of Twin-Land Oil Control Rings in Internal Combustion Engines,", *Journal of Engineering for Gas Turbines and Power*, Vol. **122,** pp. **119-129.**

Wahiduzzaman, S., Keribar, R. and Dursunkaya, Z., 1992. A Model for Evaporative Consumption of Lubricating Oil in Reciprocating Engines, *SAE Paper,* **922202**.

Yılmaz, E., Tian, T., Wong, V.W. and Heywood, J.B., 2004. The Contribution of Different Oil Consumption Sources to Total Oil Consumption in a Spark Ignition Engine, *SAE Paper,* **2004-01-2909.**

Yoshida, H., Yamada, M. and Kobayashi, H., 1995. Diesel Engine Oil Consumption Depending on Piston Ring Motion and Design, *SAE Paper,* **930995.**

Yoshida, H., Yamada, M., and Kobayashi, H., 1993. Diesel Engine Oil Consumption Depending on Piston Ring Motion and Design**,** *SAE Paper,* **930995.**

APPENDIX 1. GLIDE INPUT PARAMETERS

A.1.1. Piston and Liner Properties

Piston:

Piston Height:	116.5 mm
x – Center of Mass:	26.514 mm
y – Center of Mass:	0.142 mm
Piston Mass:	1.55 kg
Piston Moment of Inertia:	3070.24 kgmm^2
Piston Profile:	Profile is taken symmetric at TS and ATS is shown in **Figures A.1 and A.2**

Crown:

106.5 mm	-2.072 µm
116.5 mm	-2.072 µm

Skirt:

0 mm	-0.049 µm
3 mm	-0.019 µm
8 mm	-0.004 µm
25 mm	0 µm
30.5 mm	-0.002 µm
39.5 mm	-0.014 µm
65.5 mm	-0.114 µm
82.8 mm	-0.247 µm

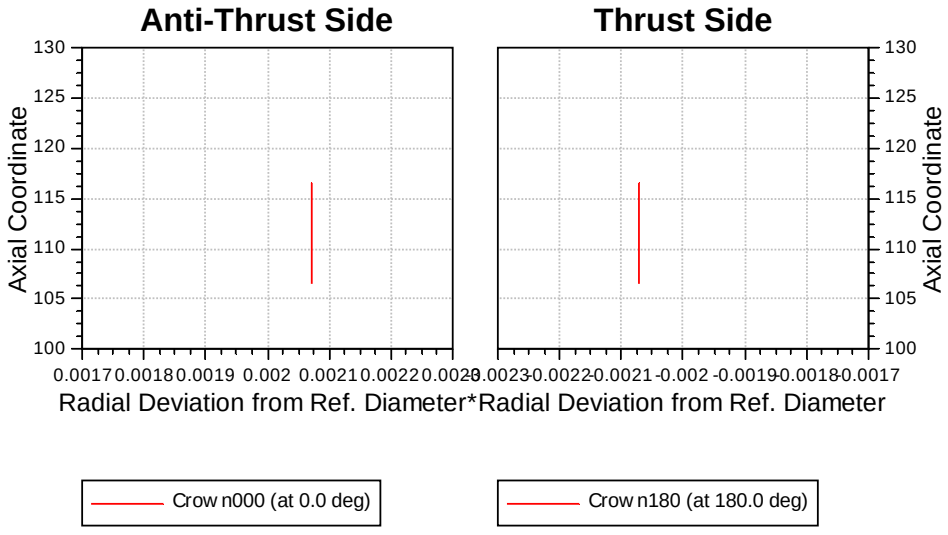

Figure A.1: Piston Top Land Profile

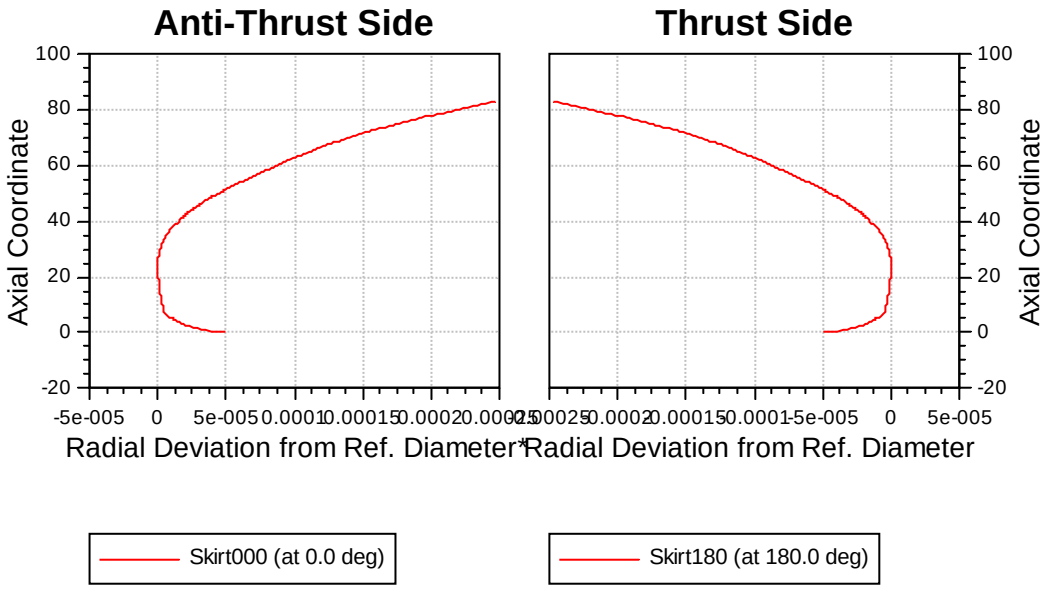

Figure A.2: Piston Skirt Profile

Liner:

Top Deck:	374 mm
Liner Height:	240.9 mm
Liner Profile:	Profile is taken symmetric at TS and ATS. **(Figure A.3)**
0 mm	20 µm
240.9 mm	20 µm

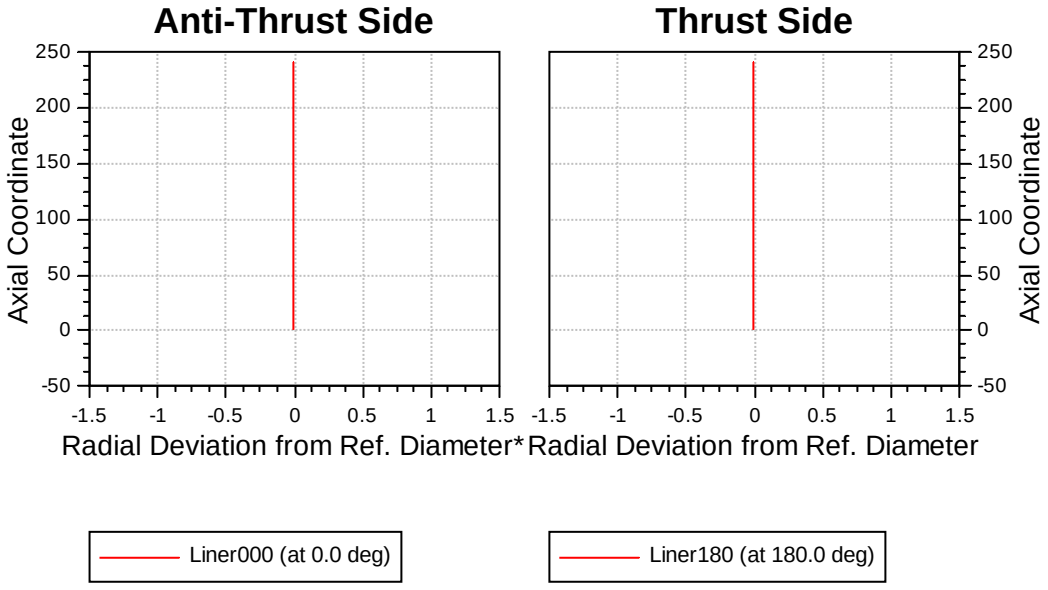

Figure A.3: Cylinder Bore Profile

Conrod:

x – Center of Mass:	-5.307 mm
y – Center of Mass:	71.656 mm
Conrod Mass:	2.89 kg
Conrod Moment of Inertia:	28152.38 kgmm^2
Big End Diameter:	125 mm
Small End Diameter:	70 mm

Piston Pin:

Pin Mass:	1 kg
Pin Moment of Inertia:	353.31 kgmm^2

A.1.2. Piston Rings and Ring Groove Properties

1. Ring (Half Keystone Ring):

Ring Mass:	31.7 g
Center of Gravity:	2.5 mm
Pre – Twist Angle:	0º
Tangential Force:	35 N
Ring End:	0.35 mm (variable)
Peripheral Edge:	0.4 mm
Summit Roughness:	0.56 μm
Radial Deviation:	-1.036 (above groove)
Radial Deviation:	-0.381 μm (below groove)
Groove Root Depth:	-5.5 mm
Distance from Piston Top:	11.555 mm
Groove Top Angle:	7.2º
Profile of Ring Face:	**(Figure A.4)**
0.05 mm	0.1 mm
0.03 mm	0.3 mm
0.0016 mm	0.5 mm
0.0006 mm	0.7 mm
0.0001 mm	0.9 mm
5e-005 mm	1.1 mm
1e-005 mm	1.3 mm
0 mm	1.5 mm
1e-005 mm	1.7 mm
5e-005 mm	1.9 mm
0.0001 mm	2.1 mm
0.0006 mm	2.3 mm
0.0014 mm	2.5 mm
0.003 mm	2.7 mm
0.005 mm	2.9mm
Profile of Top Side Face:	
0.5 mm	2.9 mm
2 mm	2.74 mm

4.6 mm 2.3 mm

Profile of Bottom Side Face:

0.5 mm 0 mm

4.6 mm 0 mm

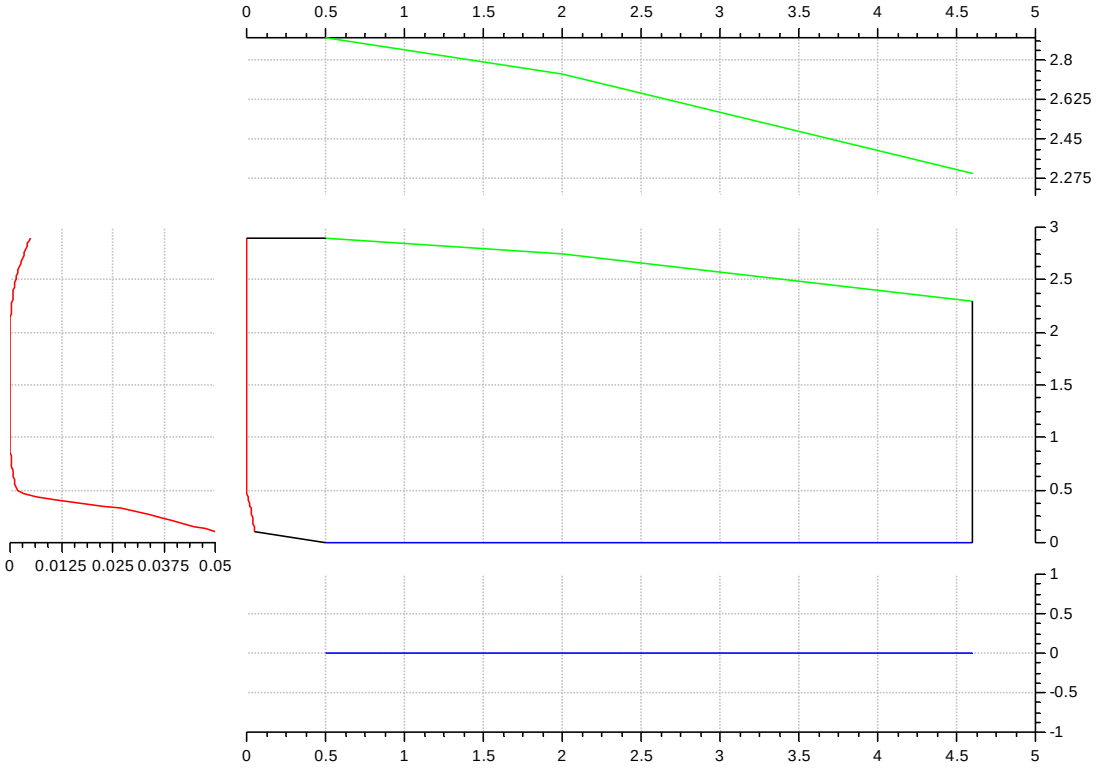

Figure A.4: First Compression Ring Profile

2. Ring (Taper Faced Ring):

Ring Mass:	29.5 g
Center of Gravity:	2.4 mm
Pre – Twist Angle:	0º
Tangential Force:	30 N
Ring End:	0.8 mm (variable)
Peripheral Edge:	0.4 mm
Summit Roughness:	0.56 µm
Radial Deviation:	-0.21 µm (above groove)
Radial Deviation:	-0.722 µm (below groove)
Groove Root Depth:	-5.75 mm
Distance from Piston Top:	25.39 mm
Groove Top Angle:	0º
Profile of Ring Face:	**(Figure A.5)**
0.001 mm	0.05 mm
0.0007 mm	0.1 mm
0.0004 mm	0.15 mm

0.0002 mm	0.2 mm
0.0001 mm	0.25 mm
3e-005 mm	0.325 mm
1e-005 mm	0.375 mm
0 mm	0.5 mm
1e-005 mm	0.75 mm
3e-005 mm	0.875 mm
7e-005 mm	0.925 mm
0.0001 mm	0.975 mm
0.0006 mm	1.25 mm
0.0016 mm	1.5 mm
0.0023 mm	1.575 mm
0.0031 mm	1.625 mm
0.0062 mm	1.75 mm
0.0158 mm	2.125 mm
0.03 mm	2.45 mm

Profile of Top Side Face:

0.2 mm	2.48 mm
4.6 mm	2.48 mm

Profile of Bottom Side Face:

0.1 mm	0 mm
4.6 mm	0 mm

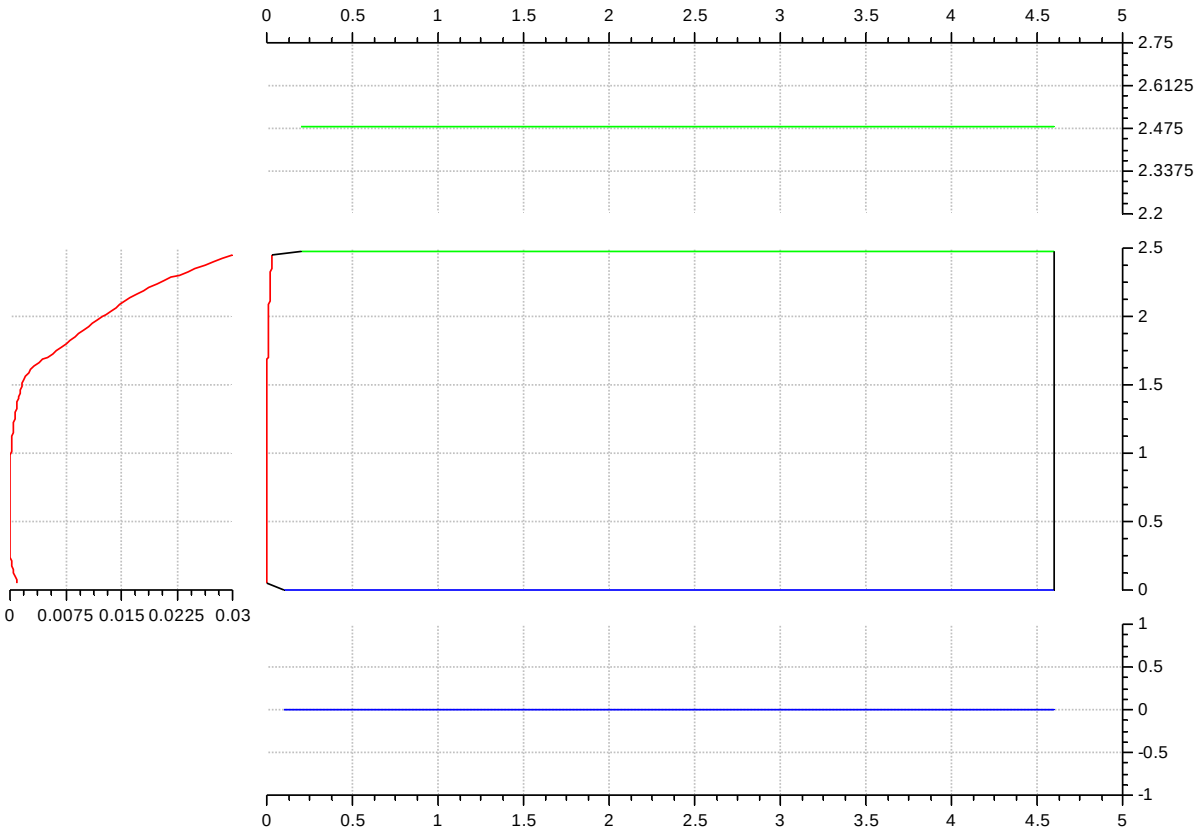

Figure A.5: Second Compression Ring Profile

Oil Ring:

Ring Mass:	19 g
Center of Gravity:	2 mm
Pre – Twist Angle:	0º
Tangential Force:	50 N
Ring End:	0.5 mm (variable)
Peripheral Edge:	0.4 mm
Summit Roughness:	0.56 μm
Radial Deviation:	-0.722 μm (above groove)
Radial Deviation:	-0.247 μm (below groove)
Groove Root Depth:	-4.725 mm
Distance from Piston Top:	33.465 mm
Groove Top Angle:	0º
Profile of Ring Face:	**(Figure A.6)**
0.2 mm	0.1 mm
0.01 mm	0.32 mm
0.0035 mm	0.35 mm
0.002 mm	0.365 mm
0.0008 mm	0.38 mm
0.00045 mm	0.4 mm
0.0003 mm	0.43 mm
0.0002 mm	0.45 mm
0.0001 mm	0.5 mm
5e-005 mm	0.65 mm
0.0001 mm	0.7 mm
0.0002 mm	0.75 mm
0.0003 mm	0.77 mm
0.00045 mm	0.8 mm
0.0008 mm	0.82 mm
0.002 mm	0.835 mm
0.0035 mm	0.85 mm
0.01 mm	0.9 mm
0.2 mm	1.1 mm
Profile of Top Side Face:	
0.5 mm	2.98 mm
3.1 mm	2.98 mm
Profile of Bottom Side Face:	
0.5 mm	0 mm
3.1 mm	0 mm

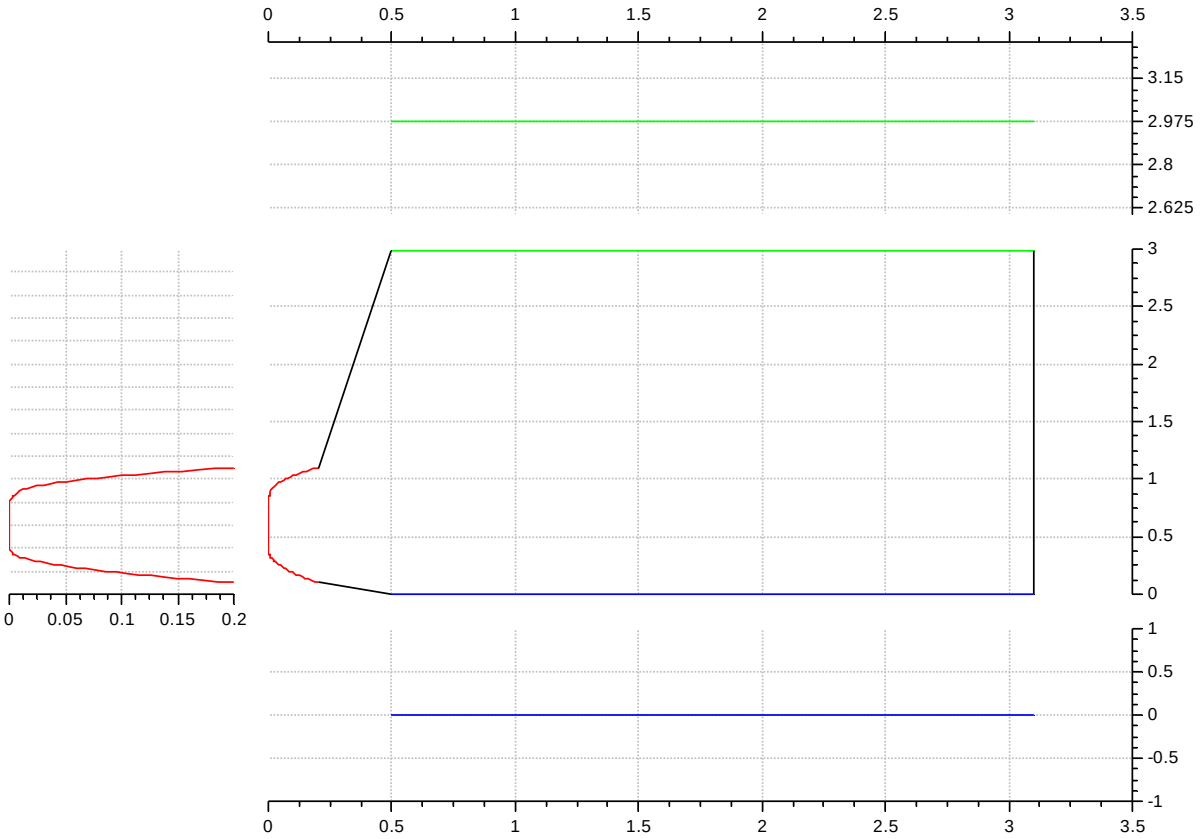

Figure A.6: Oil Ring Profile

APPENDIX 2. TECHNICAL SPECIFICATIONS OF MEASURING DEVICES

A.2.1. Technical Specifications of V&F Twin MS

Mass range	:0 – 500 amu
Resolution	:< 1 amu
Analysis time	:10 – 6500 msec/amu
Measuring range	:10^4
Cycle time gas flow	:< 250 msec
Response time	:T90 < 30 msec
Lower detection limit	:< 1 ppb Benzene
Drift	:< ± 5% per 12 h (1ppm Benzene)
Reproducibility	:< ± 3 % (1ppm Benzene)
Precision	:< ± 2 % (1ppm Benzene)
Ambient Temperature	:20°C – 40°C
Temperature change	:max. 1°C / h
Humidity	:80 % max. (none condensing)
Gas Inlet temperature	:80 – 190°C
Gas consumption	:30 – 250 ml/min, adjustable
Power	:220 V / 50 Hz or 115 V / 60 Hz, 1250 W
Dimensions	:590 x 650 x 1000 mm
Weight	:125 kg

A.2.2. Technical Specifications of AVL GU12P Uncooled Piezosensor

Measuring range	: 0-200 bar
Nominal sensitivity	: 15 pC/bar
Linearity	: <+/- 0.3% FSO
Natural frequency	: 130 kHz
Acceleration sensitivity	: 0.001 bar/g
Operating temperature limit	: 400 °C
Cyclic temperature drift	: +/- 0.6 bar
Max zero-line gradient	: 1.5 mbar/ms
Permanent zero-line deviation	: 2 bar
IMEP stability	: < 3%

BIBLIOGRAPHY

Göktan Kurnaz was born in Adana in 1982. He continued his primary education in several places and finalized in Namazgah İlköğretim Okulu in Bursa. He finished high school in Kartal Köy Hizmetleri Anadolu Lisesi in Istanbul and he had his graduate degree from Middle East Technical University in 2004 in Ankara. He has been working for Ford Otomotiv San. A.Ş. for the last three years in Product Development – Engine Development Department. The areas of his interest are dynamics and vibrations of machinery, control theory and tribology.